

DISCLAIMER

This report was prepared as an account of work sponsored by an agency of the United States Government. Neither the United States Government nor any agency thereof, nor any of their employees, makes any warranty, express or implied, or assumes any legal liability or responsibility for the accuracy, completeness, or usefulness of any information, apparatus, product, or process disclosed, or represents that its use would not infringe privately owned rights. Reference herein to any specific commercial product, process, or service by trade name, trademark, manufacturer, or otherwise does not necessarily constitute or imply its endorsement, recommendation, or favoring by the United States Government or any agency thereof. The views and opinions of authors expressed herein do not necessarily state or reflect those of the United States Government or any agency thereof.

PISCES Program*

**Progress Report for 1991-1992
on
Plasma-Materials Interactions and
Edge-Plasma Physics Research**

**Principal Investigators:
R.W.Conn and Y.Hirooka**

UCLA July, 1992

*Supported by the U.S. Department of Energy under grant #DE-FG03-86ER-52134.

This report has been contributed by the PISCES team at UCLA:

Research Staff

R.W.Conn (PI)
Y.Hirooka (PI)
L.Schmitz
R.Doerner
G.Tynan
M.Khandagle
Y.Ra
R.Boivin

Support Staff

T.Sketchley
G.Gunner
S.Keller
L.Chousal
P.Luong
H.Tran
M.C.Srinivasan
H.Sasanpour

Graduate Students

R.Lehmer
Y.Tao
L.Blush
P.Chia

and collaborations have been done with:

Tokamak laboratory at UCLA: R.J.Taylor and P.Pribyl,
North Carolina State Univ.: M.Bourham, W.E.Eddy and J.Gilligan,
Sandia National Laboratory, Livermore: R.A.Causey,
Argonne National Laboratory: J.Brooks and A.Hassanein,
National Institute of Fusion Science, Japan: A.Sagara,
Japan Atomic Energy Research Institute: M.Araki and S.Tanaka.

MASTER

TABLE OF CONTENTS

	Page
1. PISCES Program	
1-1. Objectives of the program	i
1-2. Staff in the PISCES team	ii
1-3. Highlights in the program history	iii
1-4. Collaboration with other institutions	iv
1-5. List of publications	v
2. PISCES Facilities	
2-1. PISCES-A facility	2
2-2. PISCES-B Mod. facility	4
2-3. PISCES-C facility	8
2-4. PISCES-Upgrade facility development (ITER-R&D)	10
2-5. Fast scanning probe	12
2-6. Spectroscopic diagnostics	14
2-7. Laser-Induced Florecence	16
2-8. SEM & EDX facility	19
2-9. Thermal desorption facility	21
2-10. Computer data acquisition system	23
3. PISCES Experiments: Materials and Surface Physics	
3-1. Evaluation of tungsten as a PFC material (ITER-R&D)	27
3-2. Actively-cooled divertor unit brazed with C-C composites	31
3-3. Impurity transport by redeposition	34
3-4. Surface topography change by long-term erosion and redeposition	37
4. PISCES Experiments: Edge Plasma Physics	
4-1. Gas target divertor simulation in PISCES-A (ITER-R&D)	41
4-2. Sheath heat transmission to an angled surface to B-field	46
4-3. Edge plasma characterization in the CCT tokamak	47
4-4. H-mode physics -I: Turbulent transport	53
4-5. H-mode physics-II: Steady-state convection	56
5. Theoretical Analysis: Edge Plasma Modelling	
5-1. H-mode physics-III: Plasma behavior in a sheared E-field	60
5-2. Electric field effects on boundary plasma transport	62

1. PISCES Program

OBJECTIVES OF THE PISCES-PROGRAM

Materials and Surface Physics

To investigate and characterize the behavior of materials under plasma bombardment



To develop materials for plasma-facing components in fusion reactors

Edge-Plasma Physics

To investigate and understand the behavior of plasmas interacting with surfaces



To develop techniques to control the plasma flow and associated heat flux to surfaces

THE PISCES TEAM AT IPFR, UCLA

Faculty Staff: Prof. R.W.Conn (Principal Investigator)
IPFR Director

Research Staff: (1) Surface physics and Materials Development:

Dr. Y.Hirooka (Principal Investigator)
Principal Institute Scientist

Dr. M.Khandagle
Postdoctoral fellow

(2) Plasma Spectroscopy

Dr. R.Boivin
Postdoctoral fellow

(3) Edge-Plasma Physics and Innovative Concepts Development:

Dr. L.Schmitz
Institute Scientist

Dr. R.Doerner
Institute Scientist

Dr. G.Tynan
Institute Scientist

Graduate Students and their Ph.D. thesis topics:

- (1) R.Lehmer; "Effect of radial electric field on electrostatic turbulence"
- (2) L.Blush; "Spectroscopy on particles in gas target divertor"
- (3) C.Ping; "Plasma transport under the influence of E-filed"
- (4) Y.Tao; "Modelling of edge plasma behavior in sheared E-field"

Support Staff: (1) Computing: M.C.Srinivasan
H.Sasanpour

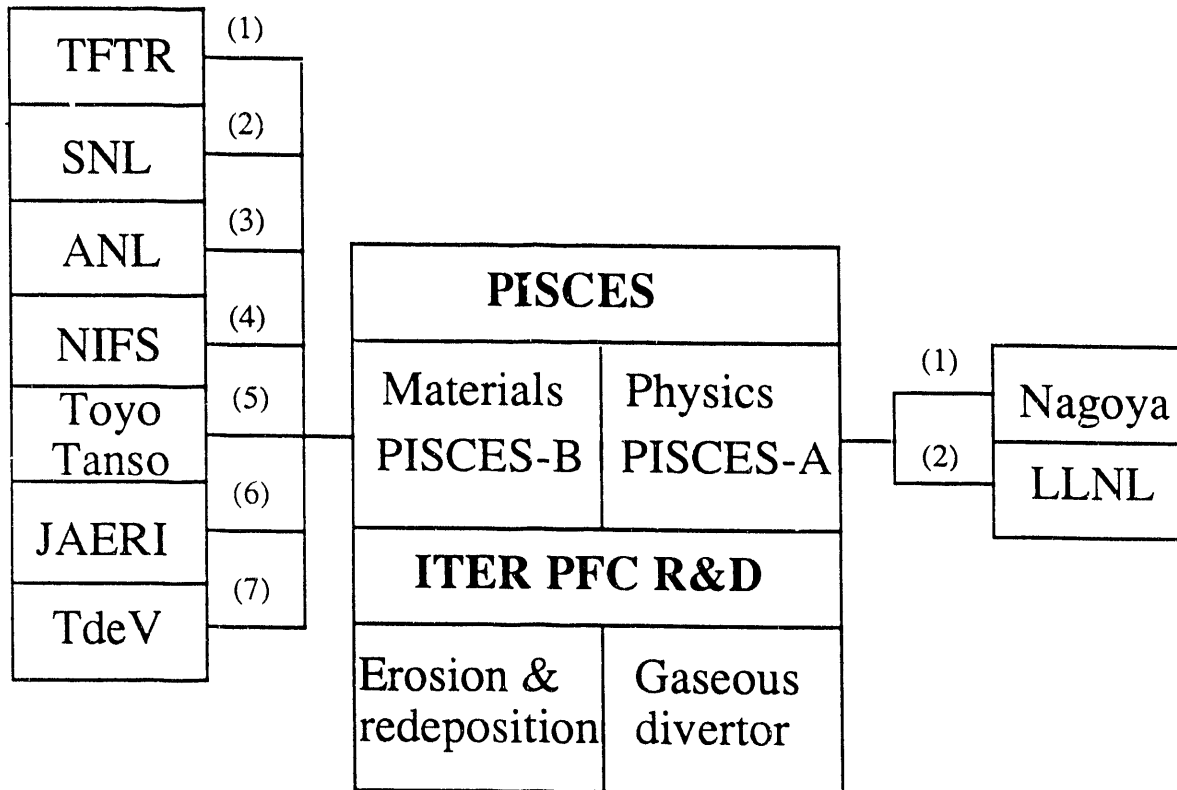
(2) Mechanical: T.Sketchley
S.Keller
L.Chousal

(3) Electrical: G.Gunner
P.Loung
H.Tran

HIGHLIGHTS IN THE PROGRAM HISTORY

- 1984** - PISCES-program funded by DOE-OFE.
* PISCES-A facility in operation.
- 1985** - First experimental demonstration of the redeposition effects in PISCES-A.
* AES-SIMS surface analysis station constructed.
- 1986** - First pump limiter simulation experiment in PISCES-A.
* Optical diagnostics established for plasma spectroscopy.
- 1987** - First off-line biased limiter ($E \times B$) experiments in PISCES-A.
* PISCES-B design started.
- 1988** - CCT experiments started in collaboration with Tokamak Lab., UCLA.
* SEM-EDX installed (UCLA-TRW laboratory).
- 1989** - First gaseous divertor experiment in PISCES-A.
- First boronized graphite experiment in PISCES-B.
* PISCES-B with in-situ AES-SIMS completed.
- 1990** - First fully poloidal measurements of plasma edge flows in CCT.
- Experimental proof of the radial electric field effect on plasma turbulence
* PISCES-C (Jr.) constructed.
- 1991** - First solid target boronization (STB) applied in the Tokamak de Varennes
- First observation of large scale dc convection patterns during L-mode in CCT
* PISCES-Upgrade design started.
- 1992** - Impurity retention measurements in gas target divertor simulation in PISCES-A
- Tungsten coatings erosion experiments in PISCES-B
* Laser-induced fluorescence diagnostics.

PISCES COLLABORATION IN 1991-1992



Materials collaboration:

- (1) DT-Materials Physics Meeting,
- (2) W-coatings: D-inventory
- (3) REDEP analysis on impurity transport exps.
- (4) RES exps. on C-C composites for LHS
- (5) Boronized C-C composite development
- (6) Actively-cooled divertor unit tests
- (7) Solid target boronization

Plasma physics collaboration:

- (1) Electron cyclotron heating exps.
- (2) Sheath heat transmission exps.

PUBLICATIONS FROM THE PISCES-TEAM

- (1) "Plasma surface interaction experimental facility (PISCES) for materials and edge physics studies"
D.M.Goebel, G.Campbell and R.W.Conn
J.Nucl.Mater. 121(1984)277.
- (2) "Observation of enhanced particle removal rates in pump limiter simulation experiments"
D.M.Goebel and R.W.Conn
J.Nucl.Mater. 129&129(1984)249.
- (3) "Large area lanthanum hexaboride electron emitter"
D.M.Goebel, Y.Hirooka and T.A.Sketchley
Rev.Sci.Instrum. 56(1985)1717.
- (4) "Large area lanthanum molybdenum electron emitters"
D.M.Goebel, Y.Hirooka and G.A.Campbell
Rev.Sci.Instrum. 56(1985)1888.
- (5) "Quasi-thermodynamic prediction of hydrogen reemission behavior from titanium films"
Y.Hirooka, D.M.Goebel and R.W.Conn
J.Nucl.Mater. 135(1985)82.
- (6) "Materials erosion and redeposition studies at the PISCES facility - net erosion under redeposition"
Y.Hirooka, D.M.Goebel, R.W.Conn, W.K.Leung and G.A.Campbell
J.Nucl.Mater. 141-143(1986)193.
- (7) "Erosion and redeposition experiments in the PISCES facility"
D.M.Goebel, Y.Hirooka, R.W.Conn, W.K.Leung, G.A.Campbell, J.Bohdansky, K.L.Wilson, W.Bauer, R.A.Causey, A.E.Pontau, A.R.Krauss, D.M.Gruen and M.H.Mendelsohn
J.Nucl.Mater. 145-147(1987)61.
- (8) "High plasma-flux elevated temperature sputtering of Cu-Li alloys"
A.R.Krauss, D.M.Gruen, M.H.Mendelsohn, R.W.Conn, D.M.Goebel, Y.Hirooka and W.K.Leung
J.Nucl.Mater. 145-147(1987)401.
- (9) "Materials surface modification by plasma bombardment under simultaneous erosion and redeposition conditions"
Y.Hirooka, D.M.Goebel, R.W.Conn, G.A.Campbell, W.K.Leung, K.L.Wilson, R.A.Causey, M.H.Morse and J.Bohdansky
Nucl. Instr. & Methods-B 23(1987)458.
- (10) "Behavior of graphite under heat load and in contact with a hydrogen plasma"
J.Bohdansky, C.D.Croessmann, J.Linke, J.M.McDonald, D.H.Morse, A.E.Pontau, R.D.Watson and J.B.Whitley, D.M.Goebel, Y.Hirooka, K.Leung, R.W.Conn, J.Roth, W.Ottenberger and H.E.Kotzlowsky
Nucl.Instr. & Methods-B 23(1987)527.

- (11) "Temperature and composition dependence of the high flux plasma sputtering yield of Cu-Li binary alloys"
A.R.Krauss, M.H.Mendelsohn, D.M.Gruen, R.W.Conn, D.M.Goebel, Y.Hirooka, W.K.Leung and J.Bohdansky
Nucl.Instr. &Methods-B 23(1987)511.
- (12) "Hydrogen pumping and release by graphite under high flux plasma bombardment"
Y. Hirooka, W. K. Leung, R. W. Conn, D. M. Goebel, B. LaBombard and R. E. Nygren
J. Vac. Sci. & Technol.-A 6(1988)2965.
- (13) "Erosion of graphite by high flux hydrogen plasma bombardment"
D. M. Goebel, J. Bohdansky, R. W. Conn, Y. Hirooka, B. LaBombard, W. K. Leung, R. E. Nygren, J. Roth and G. R. Tynan
Nuclear Fusion 28(1988)1041.
- (14) "Deuterium pumping and erosion behavior of selected graphite materials under high flux plasma bombardment in PISCES-A"
Y.Hirooka, R.W.Conn, D.M.Goebel, B.LaBombard, W.K.Leung, R.E.Nygren and Y.Ra
J.Nucl. Mater. 163-165(1988).
- (15) "Erosion and Redeposition Behavior of selected NET-candidates under high-flux plasma bombardment in PISCES-A"
E.Franconi, Y.Hirooka, R.W.Conn, B.LaBombard, W.K.Leung and R.E.Nygren
J.Nucl.Mater 163-165(1989).
- (16) "Presheath profiles in simulated tokamak edge plasmas"
B.LaBombard, R.W.Conn, Y.Hirooka, R.Lehmer, W.K.Leung, R.E.Nygren, Y.Ra, G.Tynan
J.Nucl.Mater. 162-164 (1989)314.
- (17) "Erosion and redeposition of graphite by hydrogen plasmas"
D.M.Goebel, J. Bohdansky, R.W. Conn, Y. Hirooka, B. LaBombard, W. K. Leung, R. E. Nygren and G.R.Tynan
Fusion Technol. 15(1989)102.
- (18) "An in-situ spectroscopic erosion yield measurement and its applications to sputtering and surface morphology alterations"
W.K.Leung, Y.Hirooka, R.W.Conn, D.M.Goebel, B.LaBombard and R.E.Nygren
J.Vac. Sci. & Technol.-A. 7(1989)21.
- (19) "In-situ spectroscopic measurements of erosion behavior of TFTR-redeposited carbon materials under high-flux plasma bombardment in PISCES-A"
Y.Hirooka, A.Pospieszczyk, R.W.Conn, B.LaBombard, B.Mills, R.E.Nygren
Presented at 35th National Symposium of American Vacuum Society, Atlanta, 1988
J.Vac. Sci. & Technol.-A 7(1989)1070.
- (20) "Hydrogen isotope trapping on graphite collectors during an isotope exchange experiment in the Tokamak Fusion Test Reactor"
S.J.Kilpatrick, R.E.Nygren, W.R.Wampler, M.Ulrickson, H.F.Dylla, D.M.Manos, A.T. Ramsey, and Y.Hirooka
J.Vac.Sci. & Technol.-A 7(1989)1087.

- (21) "Spectroscopic studies of carbon impurities in PISCES-A"
Y.Ra, A.Pospieszczyk, Y.Hirooka, W.K.Leung, R.W.Conn
J.Vac.Sci.& Technol.-A8(1990)1783.
- (22) "A new plasma-surface interactions research facility: PISCES-B and first materials erosion experiments on bulk-boronized graphite"
Y.Hirooka, R.W.Conn, T.Sketchley, W.K.Leung, R.Doerner, J.Elvurm, G.Gunner, M.Khandagel, R.Lehmer, P.Luong, Y.Ra, L.Schmitz and G.Tynan
J.Vac.Sci.&Technol.-A8 (1990)1790.
- (23) "Radiation-enhanced sublimation of graphite in PISCES-experiments"
R.Nygren, J.Bohdansky, A.Pospieszczyk, R.Lehmer, Y.Ra, R.W.Conn, R.Doerner, Y.Hirooka, W.K.Leung, and L.Schmitz
J.Vac.Sci.&Technol.-A8(1990)1778.
- (24) "An electrostatic barrier scrape-off Layer for control of core plasma effluxes in tokamaks"
B. LaBombard, R.W. Conn, G. Tynan,
Plasma Physics and Controlled Fusion 32(1990)483.
- (25) "An Omegatron mass-spectrometer for plasma ion species analysis"
E.Y.Wang, L.Schmitz, Y.Ra, B.Labombard, R.W.Conn
Rev.Sci.Instr. 61(1990)2155.
- (26) "Bulk-boronized graphites for plasma-facing components in ITER"
Y.Hirooka, R.W.Conn, R.Causey, D.Croessmann, R.Doerner, D.Holland, M.Khandagle, T.Matsuda, G.Smolik, T.Sogabe, J.Whitely, K.Wilson
J.Nucl.Mater. 176&177(1990)473.
- (27) "Development of bulk-boronized graphites for fusion reactor applications"
T.Sogabe, T.Matsuda, H.Ogura, Y.Hirooka, M.Khandagle and R.W.Conn,
Proc. Int.Symp. on Carbon, Tsukuba, Nov. 1990, page 886.
- (28) "Evaluation of bulk-boronized graphite as a plasma-facing material in fusion devices"
Y.Hirooka, R.W.Conn, T.Sogabe, T.Matusda, H.Ogura
Proc. Int.Symp. on Carbon, Tsukuba, Nov. 1990, page 890.
- (29) "Experimental simulation of the gaseous divertor concept in PISCES-A"
L.Schmitz, R.Lehmer, G.Chevalier, G.Tynan, P.Chia, R.Doerner, R.W.Conn
J.Nucl.Mater. 176&177(1990) 522.
- (30) "Materials analysis of TEXTOR limiter tiles"
R.Doerner, B.Mills, E.Wallura, D.S.Walsh, G.Chevalier, R.W.Conn, K.H.Dipple, B.L.Doyle, H.G.Esser, K.H.Finken, D.Gray, Y.Hirooka, K.Koizlik, A.Miyahara, R.A.Moyer, J.G.Watkins, J.Winter
J.Nucl.Mater. 176&177(1990)954.
- (31) "Experimental proof of a novel RF limiter concept in PISCES-A"
T.Shoji, A.Grossman, R.Conn, Y.Hirooka, R.Lehmer, W.Leung, L.Schmitz, G.Tynan
J.Nucl.Mater. 176&177(1990)830.
- (32) "Performance of boron/carbon first wall materials under fusion relevant conditions"
J.Linke, H.Bolt, R.Doerner, H.Grübmeier, Y.Hirooka, H.Hoven, C.Mingam, H.Schlze, M.Seki, E.Wallura, T.Weber, J.Winter
J.Nucl.Mater. 176&177(1990)856.

- (33) "Chemical erosion of selected carbon-carbon composites under high-flux hydrogen plasma bombardment in PISCES-B'
A.Sagara, Y.Hirooka, R.W.Conn, A.Miyahara, G.Chevalier, R.Doerner, M.Khandagle and N.Noda
Proc. 16th SOFT conf., London, Sep. 3-7th, 1990.
- (34) "Hydrogen and deuterium plasma interactions with brazed first wall elements"
I.Smid, E.Wallura, J.Winter, H.Nickel, R.Doerner, Y.Hirooka, R.W.Conn, W.Jager, M.Grasserbauer, E.Kny, N.Rehis
Proc. 16th SOFT conf., London, Sep. 3-7th, 1990.
- (35) "Applications of SiC and B4C coat-mix material: a new candidate for plasma-facing components"
C.Mingam, R.W.Conn, F.Dias, R.Doerner, Y.Hirooka, J.Linke, H.Nickel
Proc. 16th SOFT conf., London, Sep. 3-7th, 1990.
- (36) "Enhanced confinement in CCT and PISCES-A in the presence of radial electric fields"
R.Taylor, R.W.Conn, B.Fried, R.Lehmer, J.Liberati, P.Pribyl, L.Schmitz, G.Tynan, and B.Wells
Proc. 13th Int.Cont.on Plasma Physics and Controlled Fusion Research, Washinton-DC, 1990, IAEA-CN-53/A-6-5.
- (37) "Pumped divertors and limiters for tokamaks"
R.W.Conn
Fusion Eng. and Design. 14(1991)81.
- (38) "Interactions of bulk-boronized graphites with deuterium plasmas in PISCES-B"
Y.Hirooka, R.W.Conn, M.Khandagle, G.Chevalier, T.Sogabe, T.Matsuda, H.Ogura, H.Toyoda, H.Sugai
Fusion Technol. 19(1991)2059.
- (39) "Ohmic and H-Mode Transport in the CCT Tokamak Edge Plasma"
G.R.Tynan, R.W.Conn, R.Doerner, R.Lehmer and L.Schmitz
Proc. 18th Eurpean Conf. on Controlled Fusion, Berlin 1991, D-23(III-89)
- (40) "Steady-state convection and fluctuation-driven particle transport in the tokamak H-mod transition"
G.R.Tynan, L.Schmitz, R.W.Conn, R.Doerner, R.Lehmer
To be published in Phys.Rev.Lett.
- (41) "Solid Target Boronization in the Tokamak de Varennes"
Y.Hirooka, C.Boucher, R.W.Conn, B.Gregory, M.Khandagle, E.Knystautas, T.Matsuda, R.W.Paynter, G.G.Ross, B.Stansfield
To be published in Nucl. Fusion.
- (42) "EDX, AES and XPS analysis of boronized graphites developed for plasma-facing components for fusion devices"
M.Khandagle, Y.Hirooka, T.Sogabe, T.Matsuda, R.Arghavani, and R.W.Conn
To be published Surface Science.
- (43) "Spectroscopic studies of chemical sputtering of graphite due to hydrogen and oxygen plasma bombardment"
Y.Ra, Y.Hirooka, L.Schmitz and R.W.Conn.
To be published in J.Chem.Phys.

- (44) "Evaluation of tungsten as a plasma-facing material for steady state magnetic fusion devices"
Y.Hirooka, M.Bourham, J.N.Brooks, R.A.Causey, G.Chevalier, R.W.Conn
W.H.Eddy, J.Gilligan, M.Khandagle and Y.Ra.
To be pulished in J.Nucl.Mater. (presented at the 10th PSI conf. in Monterey, 1992).
- (45) "Impurity transport and retention in a gas target divertor: simulation experiments in PISCES-A and modeling results"
L.Schmitz, L.Blush, G.Chevalier, R.W.Conn, R.Lehmer, Y.Hirooka, G.Tynan and P.Chia,
To be pulished in J.Nucl.Mater. (presented at the 10th PSI conf. in Monterey, 1992).
- (46) "Impurity transport under magnetized plasma bombardment in PISCES-B Mod."
M.Khandagle, J.N.Brooks, Y.Hirooka, A.Hassanein, Y.Ra and R.W.Conn
Submitted for publication in J.Nucl.Mater.

PISCES-A: A Versatile Facility for Plasma Edge Physics Studies

The PISCES-A facility [1] (Fig.1) is used to investigate novel divertor and plasma edge management concepts (in particular gas target divertors), as well as edge plasma turbulence and transport. The plasma source consists of a hot LaB₆ cathode with an annular, water-cooled copper anode and attached drifttube. The vacuum system includes four turbo-molecular pumps with a pumping speed of 1500 l/s each. The plasma diameter can be adjusted between 3 and 10 cm by three independent magnet coils located in the source region. The main chamber magnetic field (variable between 0.01 and 0.19 T) is produced by four water-cooled coils. The main diagnostics include: (1) motor driven water cooled Langmuir probes; (2) fast scanning probe assemblies capable of measuring radial density, floating and plasma potential, plasma flow velocities and Mach number profiles; (3) a 1.3 m Czerny-Turner monochromator with an OMA system; (4) a fast reciprocating probe for density and potential fluctuation measurements and the determination of fluctuation-induced transport; (5) several baratron and ionization gauges for neutral pressure measurements for neutral pressure measurements; (6) a CID camera; (7) an IR surface temperature monitor. A CAMAC crate with slow and fast data loggers and a Micro Vax computer system is used for data acquisition and processing.

Differential pumping is employed to achieve a neutral gas pressure of 2×10^{-4} - 10^{-2} torr in the plasma source, while keeping the main chamber pressure between 6×10^{-5} and 2×10^{-3} torr. Plasma is produced in H₂, D₂, He, and Ar gas. Plasma densities of 10^{11} - 5×10^{13} cm⁻³ in hydrogen and helium, and up to 1×10^{14} cm⁻³ in argon have been achieved. The electron temperature is in the range of 3 - 30 eV. Neutral hydrogen densities inside the plasma are determined from absolutely calibrated Ha line intensities. A Fabry-Perot etalon is used to measure the temperatures of main plasma ions, neutrals and various impurity species.

The PISCES-A chamber provides good diagnostic access. The fast scanning probe system has been extensively used for 2-D and 3-D mapping of plasma density and potential profiles during biased limiter and divertor simulation experiments and tests of magnetized probe theory and presheath measurements. The PISCES-A plasma source is presently converted for higher density hydrogen operation in order to study plasma plugging effects in the gaseous divertor regime. Pulsed operation will enable us to operate at a discharge current as high as 250 A. The differential pumping capability is increased by installing a second turbomolecular pump at the plasma source. This allows plasma production at higher pressures while maintaining high electron temperature and ionization efficiency.

[1] D.M.Goebel et al., J.Nucl.Mater. 121(1984)277.

2. PISCES Facilities

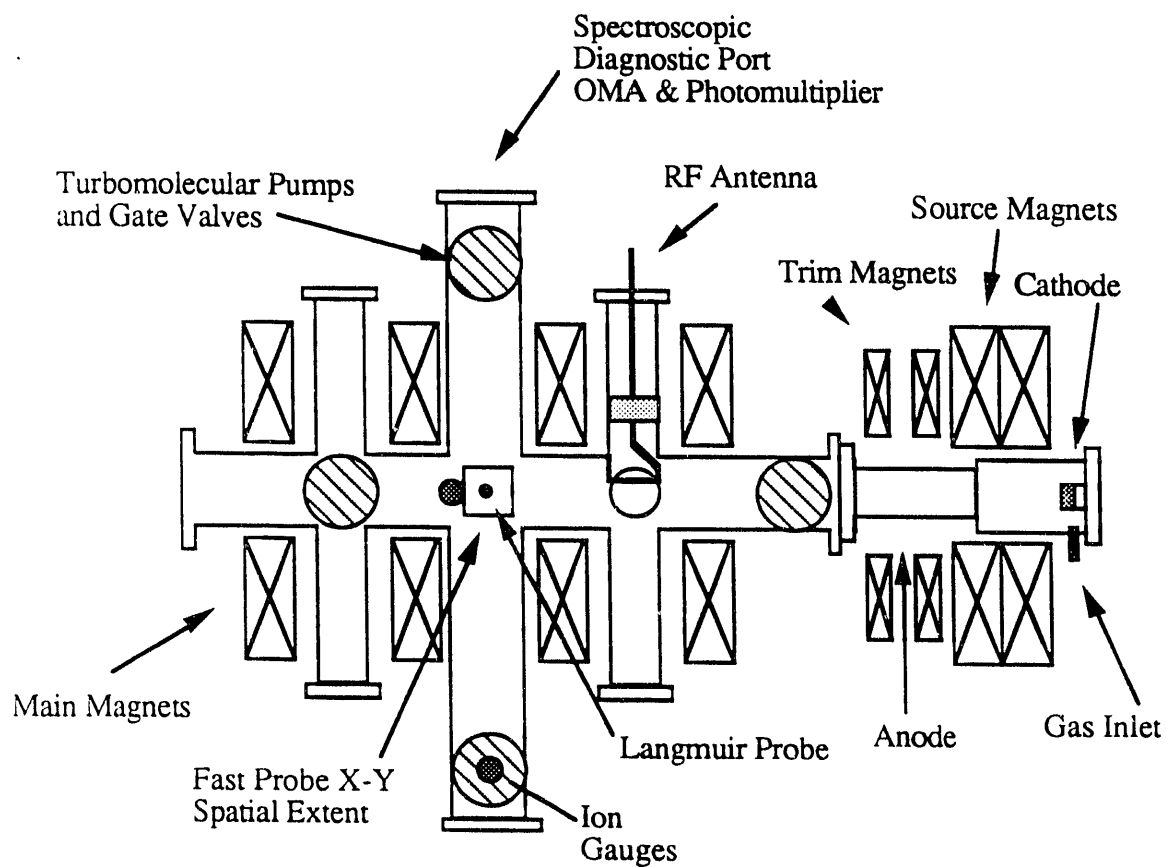


Fig. 1 The PISCES-A facility, 1992.

PISCES-B Mod.: Improved Plasma Operation for PSI-Experiments

The PISCES-B facility has been the primary off-line (non-tokamak) plasma-surface interactions research facility operating at UCLA since 1989. In 1991, the heat removal efficiency in the plasma generator of PISCES-B was modified, so that an increased heat load could be handled to sustain high-density, steady-state plasmas.

In PISCES-B Mod. the maximum plasma density achieved for the deuterium plasma is $2.5 \times 10^{13} \text{ cm}^{-3}$ and that for the argon plasma is about $1.5 \times 10^{14} \text{ cm}^{-3}$. These data are about one order of magnitude higher than those achieved in the previous plasma generator. The plasma column length and diameter are about 1 m and 6 cm, respectively. The electron temperature range explored so far is from 5 to 30 eV (see attached figure). The maximum deuterium ion bombarding flux is about $3 \times 10^{19} \text{ D-ions s}^{-1} \text{ cm}^{-2}$, close to the peak flux to the divertor plate expected in ITER, $4 \times 10^{19} \text{ D-ions s}^{-1} \text{ cm}^{-2}$ [1]. Clearly, the new regime of operation in PISCES-B Mod. is relevant to the PSI-conditions in ITER (see Table 1).

The maximum input power for plasma generation in PISCES-B Mod. is about 40 kW and is the limit of the power supply. In anticipation to increase the ion flux the power supply is currently upgraded to 100 kW as an interim solution before PISCES-upgrade is completed (The power input in PISCES-upgrade will be of the order of 1 MW).

Important diagnostics available for PSI experiments in PISCES-B Mod. are:

- (1) UHV conditions with a base total pressure of the order of 10^{-8} Torr with 6000 l/s turbo molecular and 1000 l/s titanium sublimation pumps;
- (2) 10 line-of-sight ports, focusing at the target center;
- (3) Temperature-controlled (RT-1800°C) sample probe;
- (4) two-color pyrometer for the target surface temperature measurements;
- (5) Differentially pumped residual gas analyzer (RGA) to neutral species;
- (6) In-situ surface analysis station with AES, XPS and SIMS;
- (7) CID camera with VCR;
- (8) Monochromator (0.8 and 1.3 m);
- (9) Optical multi channel analyzer (OMA) for impurity analysis;
- (10) H_{α} monitor;
- (11) Vacuum ultra-violet (VUV) spectrometer;
- (12) Slow scanning Langmuir (water-cooled) probe; and
- (13) Fast scanning Langmuir probe.

[1] T.Kuroda et al., "ITER Plasma Facing Components", ITER Documentation Series #30, IAEA, Vienna (1991).

**In-situ
AES+XPS+SIMS
analysis station**

**Main plasma
experimental
chamber**

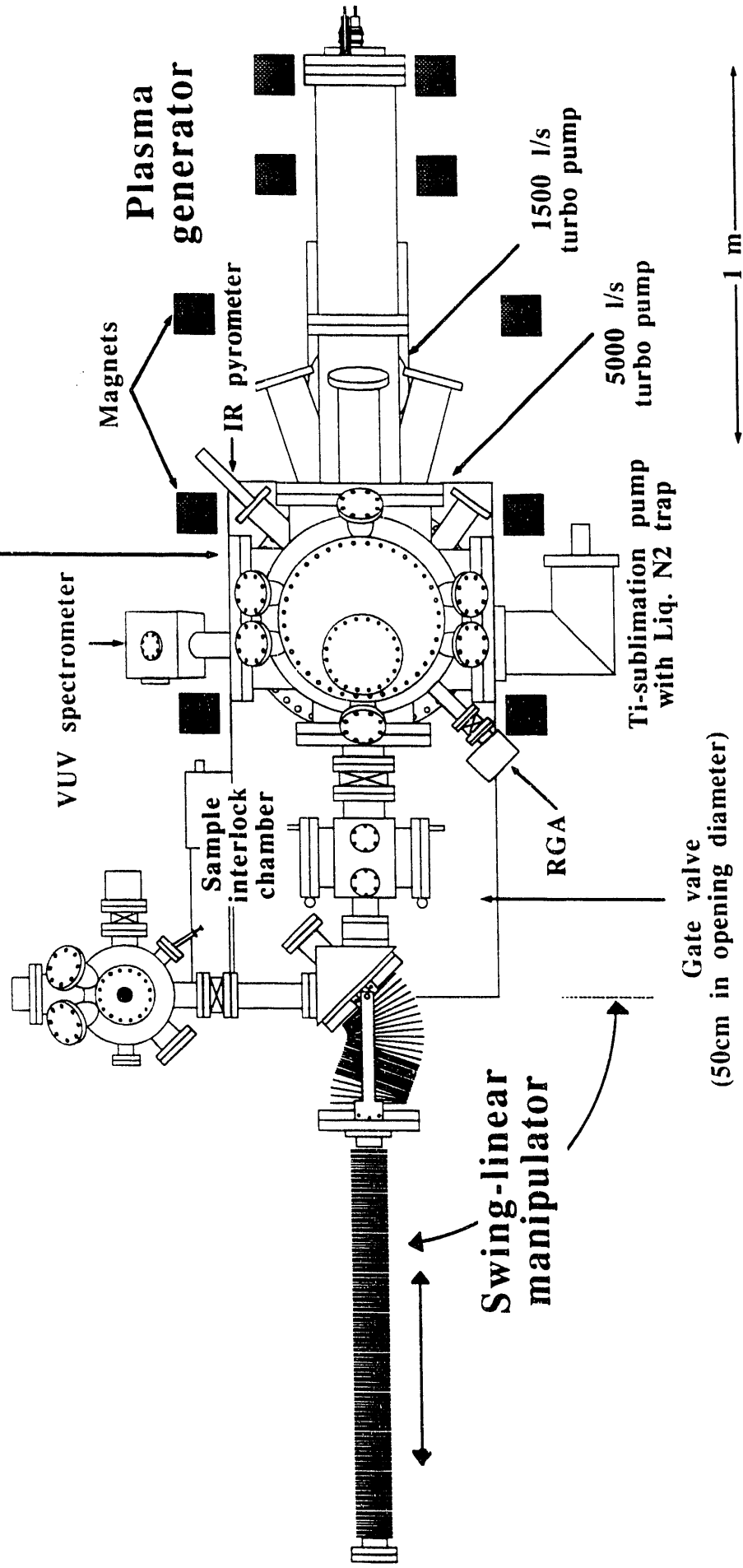


Fig. 1 The PISCES-B Mod facility at UCLA, 1992.

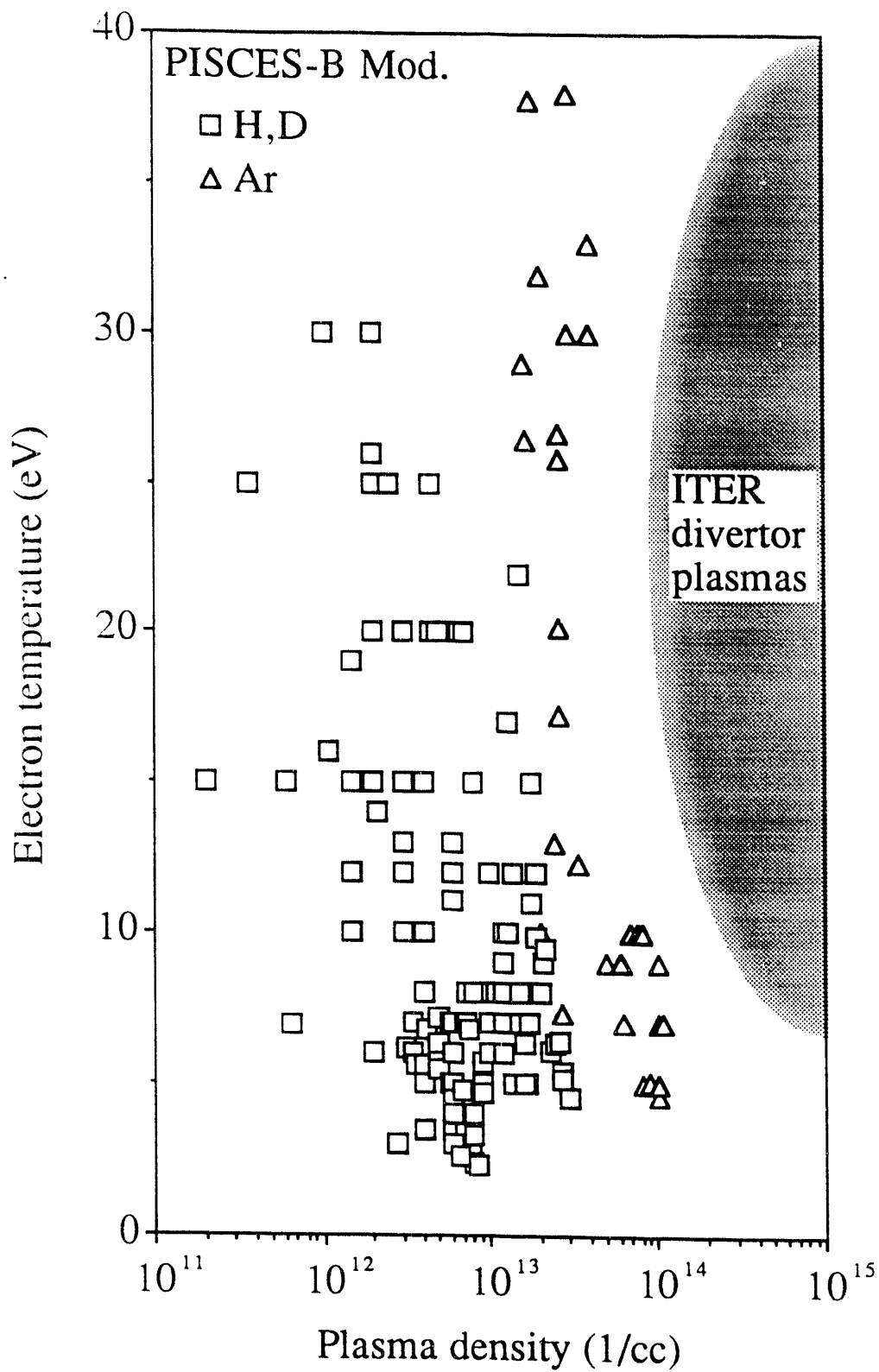


Fig. 2 Plasma operation in the PISCES-B Mod. facility.

Table PMI-conditions in PISCES-B Mod. and ITER

PMI-conditions	PISCES-B Mod.	ITER-divertor*	
Plasma species	H, D, He Ar, N	D, T, He	
Pulse duration (s)	Continuous	200	
Plasma density (cm ⁻³)	10 ¹³ (H,D) 10 ¹⁴ (Ar)	10 ¹⁴ - 10 ¹⁵	
Electron temperature (eV)	5-30	10-20	
Ion bombading flux (ions s ⁻¹ cm ⁻²)	up to 3 x 10 ¹⁹ (D-plasma)	4 x 10 ¹⁹ (peak)	
Ion bombarding energy (eV)	30 - 300 (dc bias)	60-200	
Power load (MW/m ²)	5 - 15 (with dc-bias)	10 - 30	
PFC surface temperature (°C)	RT - 1700	1000 (carbon) 1500 (tungsten)	
Ionization mean free path for 1st ionization (cm)	C** W	~ 1 ~ 0.02	~ 0.5 ~ 0.01
Neutral pressure (Torr)	up to 10 ⁻³	~ 10 ⁻²	

*From the IAEA document No.30: ITER plasma facing components.

**Physically sputtered carbon

PISCES-C Facility: A helicon wave plasma generator for PMI-experiments

PISCES-C (Jr.), a plasma-materials interaction facility using an rf plasma source, has recently been upgraded to provide continuously operating, high-density oxygen plasmas. The new setup is shown in Fig. 1. Main features of the upgraded version are:

(1) Vacuum: A wide range of operating pressures (1torr-UHV) has been achieved by using a compound molecular pump with a pumping speed of 1500 liter/sec and a UHV chamber. This provides a wide operating window of plasma parameters and a clean vacuum condition, free from contamination of the diffusion pump oil by oxygen gas.

(2) RF Plasma Source: The antenna is made of copper plates and has the geometry similar to that of the Nagoya-type III. A water-cooling line is soft-soldered on the antenna, so that the temperature and the impedance stay constant during operations. Unloaded quality factor, Q , of the antenna is aimed at around 20 with a power coupling efficiency of 70% and an amplification factor of 60. The impedance of the antenna is matched to 50Ω of the generator by two vacuum capacitors. The tuning capacitor is connected in parallel with the antenna, and the loading is in series with the generator. This setup lowers the required capacitance for matching (1100 pF for tuning and 500 pF for loading). A set of Helmholtz coils provide a magnetic field about 1KG.

(3) Diagnostics: Due to the fluctuation of floating potential by rf fields, a double probe has been built to measure plasma parameters. To prevent rf pick-up, all the connections are doubly shielded and rf chokes are used. Probe tips are made of tantalum and aligned in parallel with the magnetic field so that the drifting velocity effect can be minimized. Shown in Fig. 2 are the first plasma current data obtained by this probe (for this measurement no magnetic field was applied at the point of the probe). Also, a residual gas analyzer (RGA) is now installed to monitor neutral species. This diagnostic has made real-time process monitoring possible for plasma-materials interactions to form volatile species such as: $C + 1/2 O_2^+ = CO$ [1].

Shown in Fig. 1 is the transition behavior of plasma density (ion saturation current) observed as power input increases. Along with this transition the ionization efficiency increases by a factor of about 5, demonstrating the high ionization efficiency of helicon waves. The effect of magnetic field on plasma density is also investigated and the result is shown in Fig. 2. Clearly, the density increases linearly with increasing magnetic field, typical of plasmas generated by the helicon wave. Below 100 G ion gyro radii are larger than the pyrex tube size, resulting in a loss of plasma particle due to wall collisions.

[1] Y.Ra et al., to be published in J.Vac.Sci.&Technol.

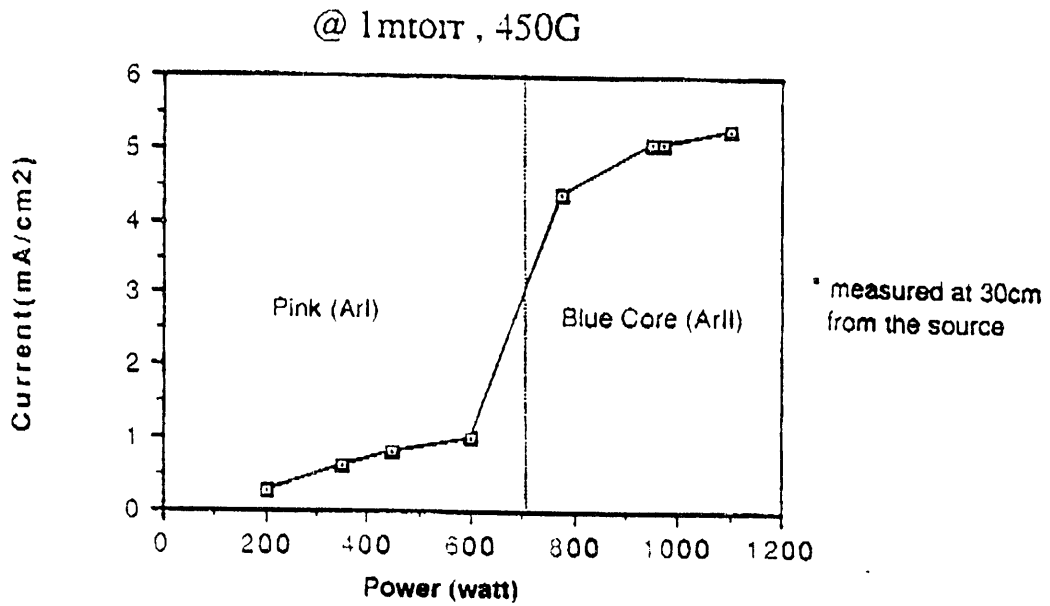


Fig. 1. Power dependence of ion saturation current

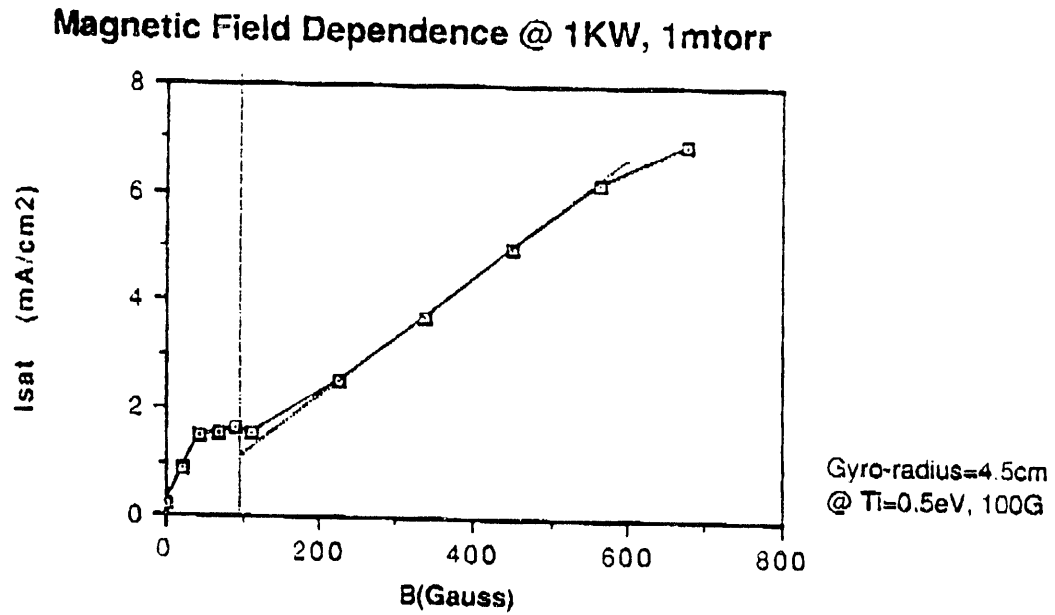


Fig. 2. Magnetic field dependence of ion saturation current

PISCES-Upgrade: A Dedicated Facility for ITER R&D on PFCs

The PISCES-Upgrade (will be referred to as PU) facility has been under design to meet the needs specified in the latest ITER R&D documents for a divertor plasma simulation facility. In particular, this facility can address the erosion/redeposition issue, specifically called out by the ITER team. The PU facility is currently designed to employ a reflex-arc discharge using lanthanum hexaboride (LaB_6) cathodes in an arrangement where the source zone is a magnetic cusp and the uniform magnetic field is 3 kG. The PU facility produces plasmas with a 176 cm^2 cross-sectional area and can fully expose component surface areas up to 350 cm^2 . The PU plasma is expected to have a density of the order of 10^{20} m^{-3} , an electron temperature of 5-20 eV, a normal plasma heat flux of 35 MW/m^2 at a -250V bias on the component test assembly, and a corresponding ion flux in the range of $4\text{-}8 \times 10^{23} \text{ m}^{-2}\text{s}^{-1}$. Components for testing can be arranged at angles to the incident B-field, and the facility will operate "steady-state".

All the PISCES-A and B devices are basically high-density, continuously operating plasma generators coupled by a magnetic field to a materials interaction region. The species of the plasma flowing into the interaction region is determined by the gas fed into the plasma generator. The ion temperature in PISCES-A and B is about a few electron volts. Therefore, if a dc bias is applied to the target, the incidence of ions is approximately normal to the surface. The electron temperature and density in PISCES can be controlled by appropriate adjustment of the discharge power, gas feed rate, and magnetic field strength. The PU facility design is based upon the operating experiences obtained in PISCES-A and PISCES-B.

The optimum geometry for high-density plasma generation comprises a short radial diffusion length coupled with a low magnetic field in the anode region. Inherent in the magnetic cusp geometry is a short anode-cathode radial separation, a large area plasma at the target location, and a region of lower magnetic field strength in the region of the anode. In a single cusp source arrangement, a magnetic cusp is formed between two large coils, and the magnetic field lines from the cusp are connected to the component test region by a long solenoid (see figure).

In addition, RF heating of ions up to energies ranging 10-20 eV is under consideration to make the plasma impact power to the target more relevant to that expected in ITER. Hot ions will make non-normal incidence of ions to the target, which can lead to a critical difference in the target sputtering behavior. Also, the application of superconducting magnets is currently evaluated.

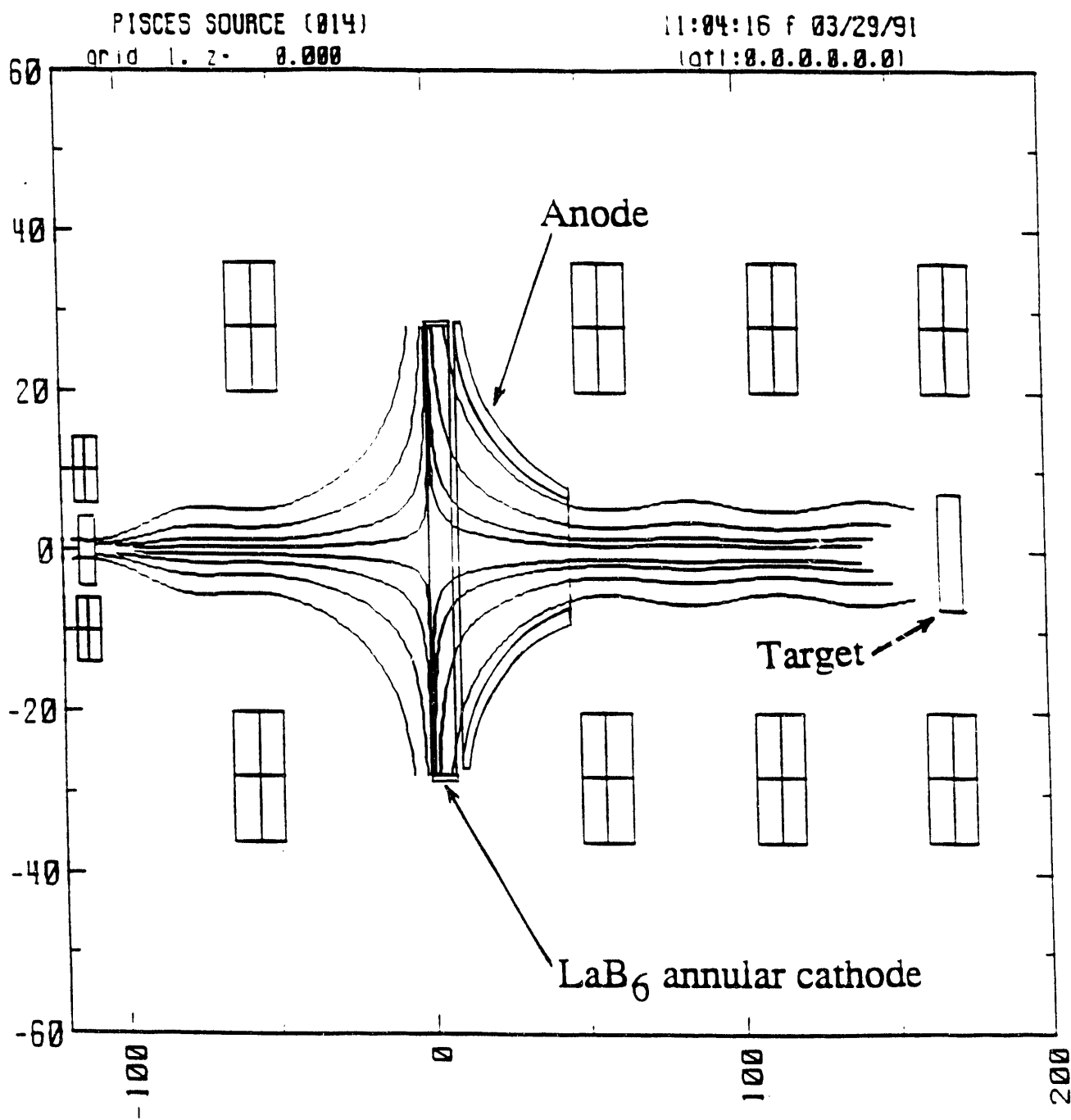


Fig. 1 The magnetic field geometry in the PISCES-Upgrade facility.

Fast Scanning Probes as Diagnostics for Steady-State Plasmas[1]

The fast scanning probe developed by the PISCES-team uses a pneumatic cylinder to drive a combination emissive and mach probe tip across the plasma column. This allows for single scan or shot profiles of the space or floating potential, density, and parallel mach number. Profiles of the space and floating potentials under identical plasma conditions can be obtained by using successive shots of the fast probe. To record the floating potential profile, the emissive probe tip is left cold. To record the space potential profile, the probe is resistively heated so that it will thermionically emit electrons into the plasma.

A schematic diagram of the probe structure is shown in Fig. 1. The fast probe actuator has a 15cm stroke and the total round trip time for the probe is 300 msec. The probe is constructed of an alumina shaft with six holes for wires to pass through. The tip is made up of five electrical probes: a loop of thoriated tungsten wire for the emissive probe, and two pairs of unidirectional probes. Each pair of unidirectional probes has one tip that faces towards the source ("upstream") and the other faces away from the source ("downstream"). One pair has tips larger than the ion Larmor radius and is referred to as a magnetized mach probe, while the other pair is smaller than the ion Larmor radius and has been used to study ion flow in plasma wakes. The parallel mach number is computed from the ratio of the currents collected by the upstream and downstream magnetized probes. Density profiles are computed from the average of the current collected by the two probes.

The fast probe diagnostic was first built for the PISCES-A facility and has been used for virtually all the edge-plasma physics experiments including: presheath profile measurements in front of material samples, the modification of the potential profiles and scrape-off layer lengths in biased scrape-off layer simulation experiments, ion flows in the wakes of probes in the plasma, modification of density profiles in RF limiter/divertor simulation experiments.

Also, a fast scanning double probe has been built for materials experiments in the PISCES-B facility. During the fast probe stroke, the probe tip voltage will be swept rapidly. This results in a number of Langmuir probe traces at different radii. These traces can be fitted automatically by the data acquisition system to produce a discrete spatial profile of electron temperature and density across the plasma column. Also, the use of the fast probe in PISCES-B material experiments will minimize sample contamination resulting from sputtered probe materials. This is important because under plasma bombardment the surface modification can readily be triggered by trace amount of impurities [2].

[1] R. Lehmer et al., UCLA-Report# UCLA-PPG-1228 (1989).

[2] Y.Hirooka et al., Nucl. Instr. & Methods-B 23(1987)458.

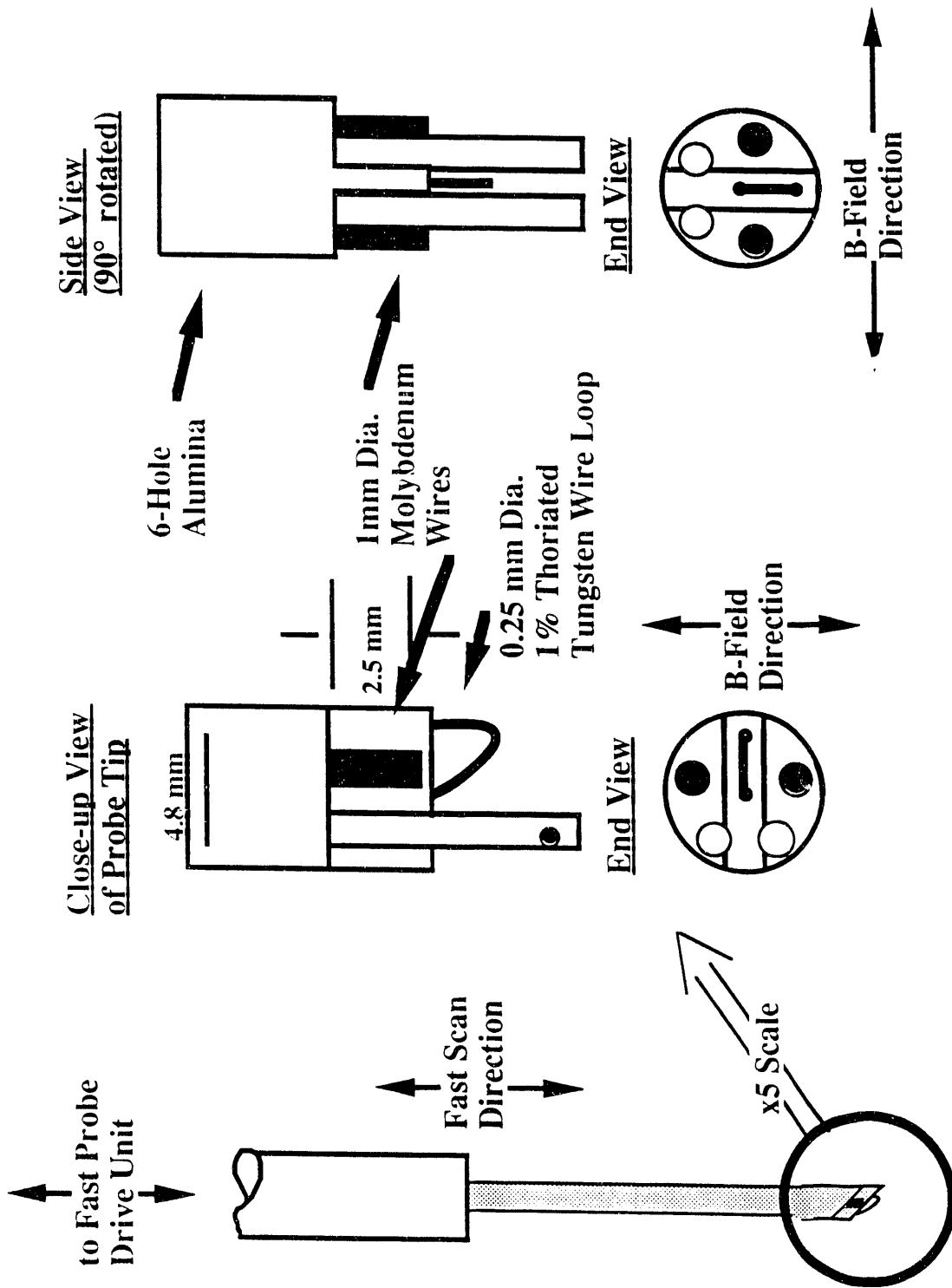


Fig. 1 Schematic illustration of fast injection probe electrodes.

Spectroscopic diagnostics for PISCES A, B and C(Jr.) Facilities

Spectroscopic techniques have been applied in the PISCES A, B and C (Jr.) facilities in diagnosis of material erosion yields [1], surface temperature profile [1], hydrogen recycling [2], impurities[3], neutral and ion temperatures and densities [4] and chemically reactive RF plasmas [5]. In addition to its uniqueness as an in-situ erosion yield measurement in material experiments, spectroscopic techniques have emerged as an integral part of plasma physics experiments.

Spectroscopic diagnostic instruments available in the PISCES Laboratory include a 1.3M Czerny-Turner spectrometer, a 0.5M Crossed Czerny-Turner spectrometer, an OMA (Optical Multi-channel Analyzer) system, a CID camera with a computer image analysis system. Also, a 0.3 M Crossed Czerny-Turner VUV spectrometer has recently been installed on the PISCES-B facility.

As to applications of these instruments, for example, OMA can be used along with spectrometers to obtain both spectral and spatial information of plasma impurities. The CID camera can be used to obtain spatial emission profiles or can produce spectral and spatial profiles simultaneously when integrated with the spectrometers. These arrangements have been made possible by efforts in the laboratory to bridge between separate instruments with customized computer software.

Because of its applicable wavelength range (between 105nm and 60 micrometers), VUV is particularly suited to study materials containing carbon and/or boron such as boronized graphites and C-C composites (see Fig. 1). The OMA system is integrated with this spectrometer to obtain emission lines of carbon and boron on the same spectra allowing direct comparison between these elements (see figure 1).

In addition to these instruments, a 10 m Å limit resolution Fabry-Prot interferometer has recently been installed on the PISCES-A facility. This interferometer is currently used in conjunction with spectrometers to increase resolution. Using the improved resolution, direct spectroscopic measurements are planned to analyze the neutral temperature in argon plasmas in PISCES-A.

[1] Y.Hirooka et.al. Fusion Technol. 19(1991)2059.

[2] R.Doerner et.al. J.Nucl.Mater. 176&177(1990)954.

[3] W.K.Leung et. al. Bull. Am.Phy.Soc. 31 (1986)

[4] L.Schmitz et. al. J.Nucl. Mater. 176&177(1990)522.

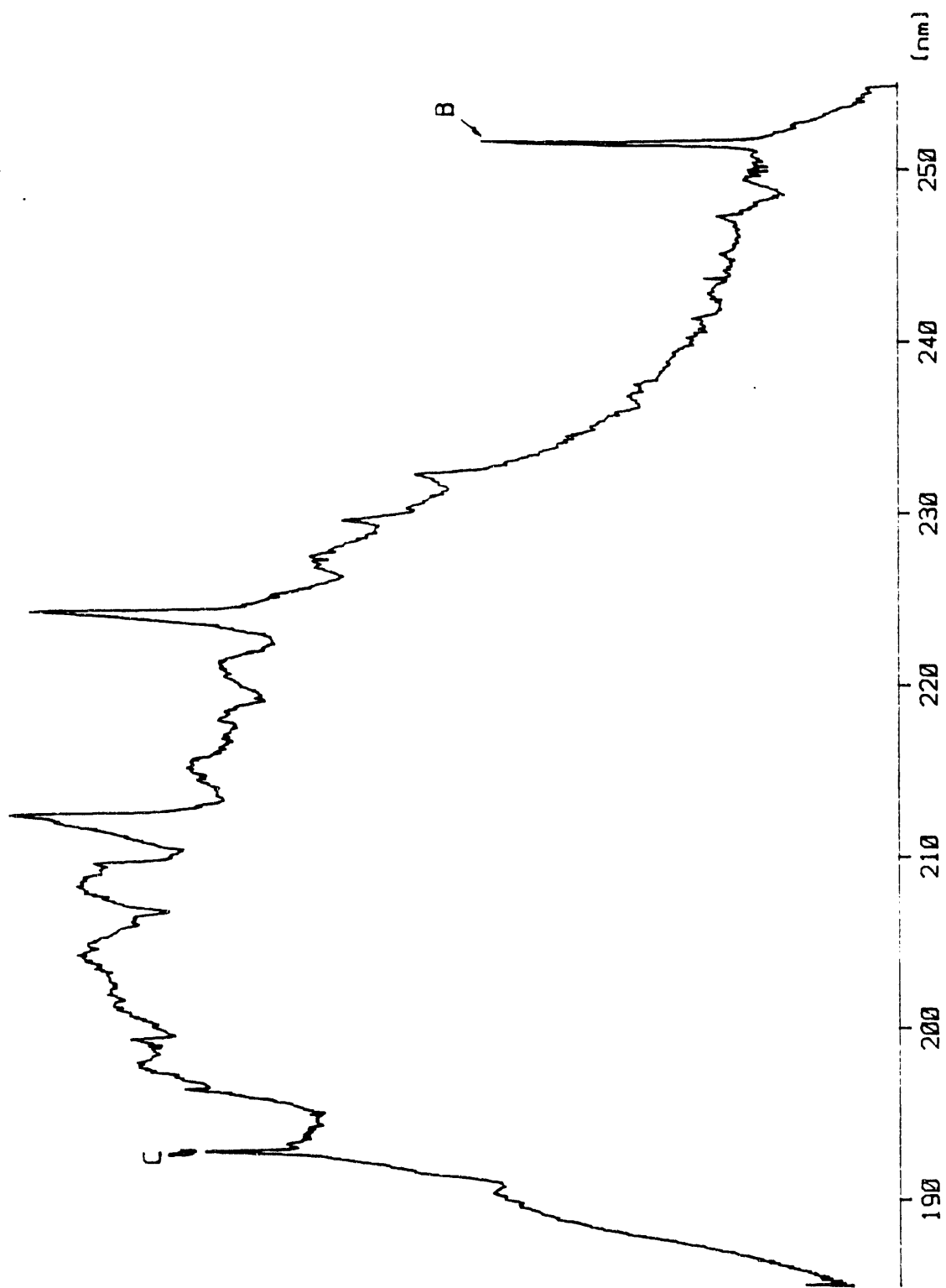


Fig. 1 Emission spectra from OMA

Laser-Induced Fluorescence Diagnostics for PISCES

Laser-induced fluorescence (LIF) is a powerful plasma diagnostic which has been used to measure: charged particle densities, velocity distributions, gas temperature and electric fields [1,2]. The LIF diagnostic system generally consists of a tunable dye laser and a spectroscopic detector. The laser is tuned to a selected transition of the particle species to be detected and then focused on a small observation volume. The laser-induced fluorescence from the excited particles is analyzed with a monochromator with channeltron or multichannel analyzer. Major advantages of LIF diagnostics are: (1) selectivity; (2) sensitivity; (3) spatial and temporal resolution; (4) independence of the knowledge of other plasma parameters; and (5) absence of stray line problems.

The laser system at the PISCES laboratory is featured with a cw tunable dye laser (Coherent model 599) with a cw argon ion pump laser (Coherent model innova 70). The output of the laser system is determined by the pump laser output, the dye conversion efficiencies (5 to 30%) and the alignment of the optical cavity. Typically, a 5 watt output pump laser will generate power ranging from 0.1 to 0.9 watt for the cw tunable dye laser. The broad tuning range made available by using different dyes enables one to cover the entire visible range (see Fig. 1). The laser can be tuned with a birefringent filter. If needed, wavelength coverage and power output can be increased by upgrading the pump laser. The typical linewidth across the spectrum of use is 40 GHz ($8 \times 10^{-5} \lambda$) but this linewidth can be substantially reduced by using a specific etalon optic system [3]. Ultimate achievable linewidths are in the order of 20 MHz ($5 \times 10^{-8} \lambda$).

By focusing the laser on a specific volume one can obtain a power density sufficient to saturate the excitation level of atoms (or molecules) of interest. Once saturated, the population of the excited level is only proportional to the fluorescence intensity and to the ground level ion population. Importantly, under these conditions the intensity of LIF is independent of the primary laser intensity. Therefore, as long as the saturation condition is met, fluctuation of laser output will not affect ion density measurements.

Fortunately, most materials presently considered for plasma-facing components can be analyzed with LIF. Although several metals have their resonances line in the UV range [4], it is possible to obtain UV dye laser output. Using LIF one can also measure the ion temperature from the Doppler effect on LIF. The Doppler broadening of the fluorescence lines is due to the thermal motion of the emitting atoms. Assuming that a local thermal equilibrium is established, the Doppler width $\Delta\nu_D$ of the fluorescence line emission (central frequency ν_0) is related to the ion temperature, T_i , in the following manner:

$$\Delta v_D = (8 \ln 2 T_i v_0^2 / m_i c^2)^{1/2}$$

where m_i and c are the ion mass and the speed of light, respectively.

Furthermore, it has been demonstrated [5] that if one uses a laser incident on a highly reflective electrode, both incident and reflected laser beams would cause fluorescence. For ions moving toward the electrode, the incident beam is shifted to red, while the reflected beam is shifted to blue. Consequently, if the ions have a net drift velocity v_d , the fluorescence line shape will have peaks at two distinct frequencies separated by a frequency interval proportionnal to v_d . This technique based on the Doppler shift enables absolute measurements of the drift velocity in a plasma. This technique has a potential to provide important information on plasma surface interactions although this possibility must be explored experimentally. The different ionic parameter measurements are summarized in Fig. 2.

Currently, the LIF system is being examined for characterizing RF-plasmas in the PISCES-C facility and will be used as a routine diagnostic for PISCES-A and B. Also, this cw laser system can be used for laser-assisted CVD of tungsten and possibly beryllium, the processes of which are under investigation. Because generally CVD processes can form high-density coatings, as opposed to plasma spray techniques, the LI-CVD may be used for in-situ repair for damaged plasma-facing components. The feasibility check experiments are under way.

-
- [1] D.E.Post and R.Behrisch (ed.) "Plasma Wall Interactions in Controlled Fusion", Plenum Press, New York (1986)
 - [2] B. Leblanc and B.L. Stansfield Phys. Rev. A27 (1983) 3279.
 - [3] Coherent Laser Technical Data (1992)
 - [4] E. Hintz J. of Nucl. Mater. 93 & 94 (1980) 86-95.
 - [5] M.J.Goeckner et al., to be published in Phys. of Fluids.

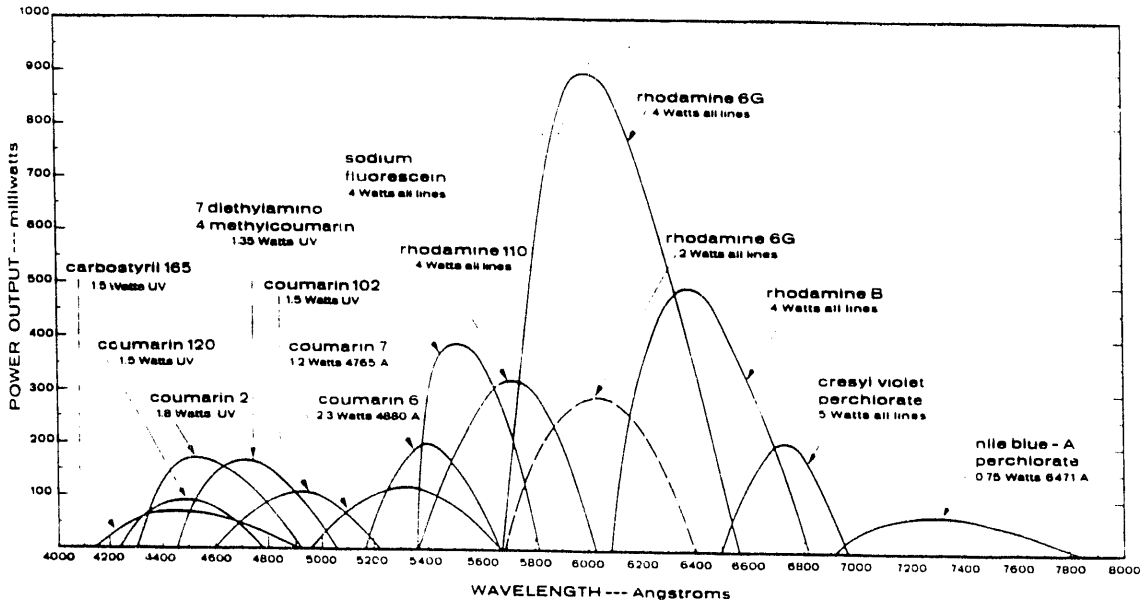


FIG. 1 Dye laser output curves of some common laser dyes. Figures below the dye indicate the typical pump power from an argon ion laser required to achieve the tuning curves shown [6].

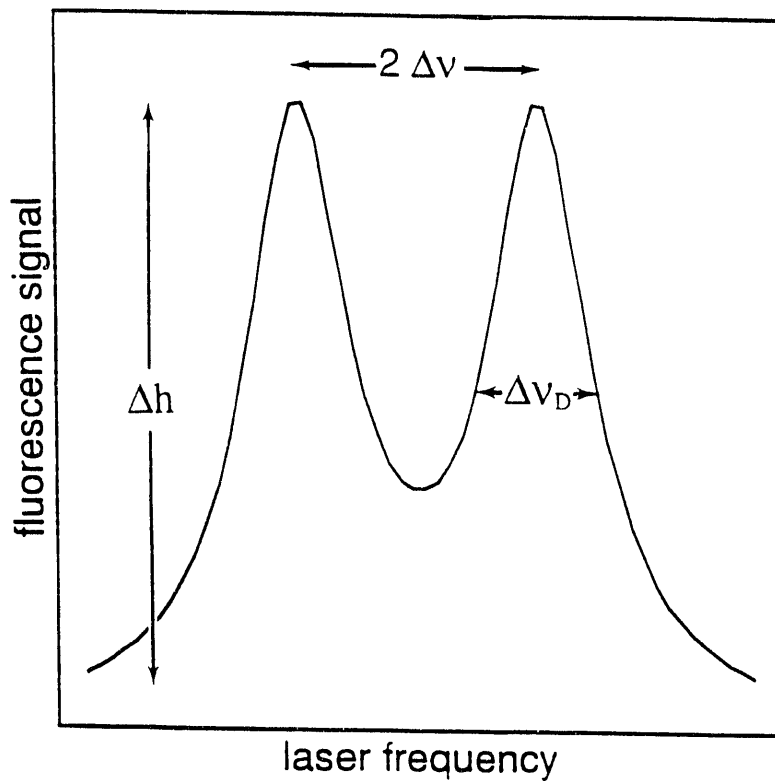


FIG. 2 By using proper calibration, the height of the fluorescence peaks will give us the ion density; the width of the peaks are related to the ion temperature and peak separation is proportional to the drift velocity.

SEM-EDX Facilities (UCLA-TRW Laboratory)

Materials for plasma-facing components like boronized graphite and C-C composites are being routinely analyzed in the PISCES laboratory using Scanning Electron Microscopy (SEM) using the JEOL T-330A, and Energy Dispersive X-ray Analysis (EDX) using the KEVEX DELTA CLASS IV system.

The boron $K\alpha$ line at 0.185 keV is very difficult to detect because it has a very low excitation probability and, at the same time, a very high probability of being absorbed in the sample matrix on emission¹. Also, the B $K\alpha$ line lies at the edge of the electronic noise of the Kevex X-ray detector so that a part of the peak is lost in the noise. Further, in case of boronized graphite, the B $K\alpha$ (0.185 keV) and C $K\alpha$ (0.282 keV) peaks overlap since the FWHM for the Kevex system is 160 eV. With these limitations, the system has been optimized to detect boron from boronized graphite having a boron concentration greater than 3%.

Using pure boron (99.9%, Cerac), pure Graphite (POCO) and B_4C as reference materials, the calibration curve has been obtained for boron concentration in boronized graphites as shown in figure 1. The offset seen for 0% B arises due to the B and C peak overlap in the EDX spectra.

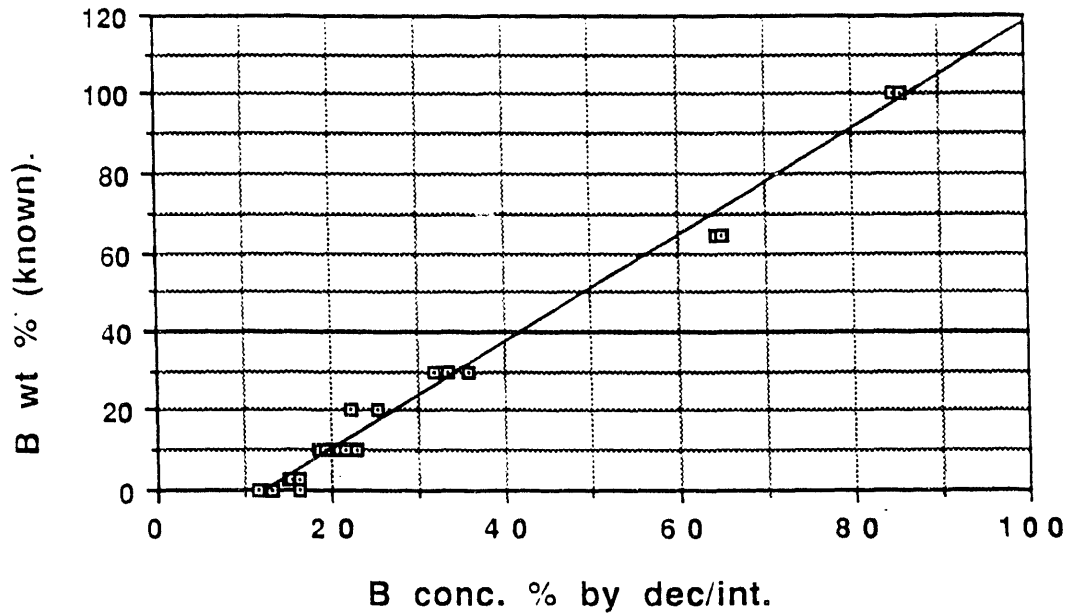
For standard based analysis, a Faraday cup is used to measure the electron beam current. Analysis is done using the deconvolution technique [1] so as to account for the distortion of the boron peak due to the electronic noise. The Kevex Quantex software is used to apply ZAF corrections to the 'k' ratios* obtained using reference deconvolution, and determine the percent atomic as well as weight concentration of B in boronised graphite. Figure 2 shows the analysis results for a number of samples using the standard based technique. The scatter in the data is probably due to variation in the boron concentration from sample to sample.

Another important feature of the Kevex EDX system is the availability of X-ray mapping, i.e. the areas of the sample where boron is concentrated can be determined. This feature is especially useful for the analysis of two-phase materials such as boronized graphites. A comparative study of EDX and other techniques such as AES and ESCA is being conducted [2] on the analysis of boronized graphites and carbon-carbon composites.

* 'k' ratio is the ratio of the peak intensity of the sample to the peak intensity of the reference standard.

[1] 'Kevex Quantex Software Reference Manual.' Kevex Instruments 1985.

[2] M.Khandagle, to be published in Surface Science.



$$B \text{ (known)} = -16.662 + 1.3397 B \text{ (dec/int).}$$

Figure 1: Calibration curve for Boron by dec/int.

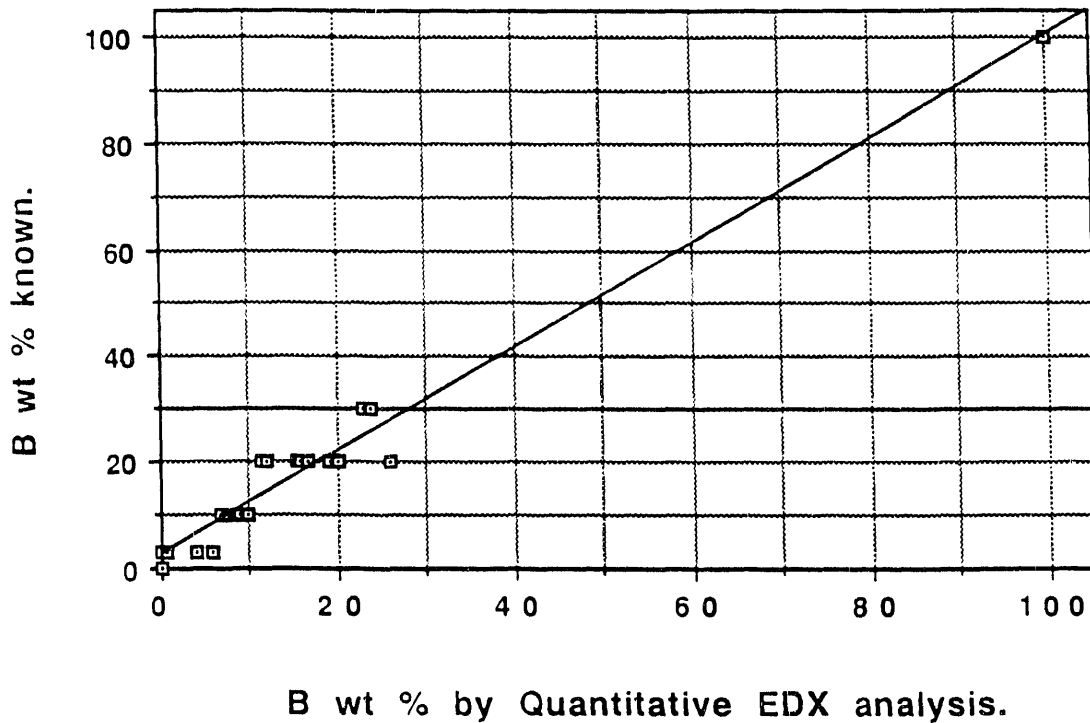


Figure 2: Results for B concentration by quantitative EDX analysis.

Vacuum Outgassing Facility for Thermal Desorption Spectrometry [1]

It is widely recognized that outgassing from plasma-facing components in tokamaks can significantly affect the performance of plasma confinement. Therefore, it is of considerable importance to study the outgassing behavior of materials using off-line facilities. The thermal desorption spectrometry (TDS) technique is widely used to measure outgassing characteristics of materials.

To perform outgassing measurements a dedicated UHV system was constructed first in 1988 and then upgraded in 1990. A schematic diagram of this outgassing facility is shown in Fig. 1. Major components are: (1) 6-way cross stainless steel chamber; (2) BA-gauge; (3) a turbomolecular pump with a pumping speed of 170 l/s; (4) a residual gas analyzer (RGA) with a PC-data acquisition system; and (5) a computer-controlled infrared (IR) furnace.

In this outgassing facility, a test sample can be heated by the IR-furnace from room temperature to temperatures around 1000°C typically at a rate of around 20 deg/min. During the course of thermal desorption measurement, partial pressures of desorbed gases are monitored with the RGA system.

As an example, the thermal desorption spectra from a bulk-titanized graphite sample are shown in Fig. 2. The total amount of desorbed gasses is calculated from the time-integration of their partial pressures. In this case, the total amount of gas desorption is evaluated to be 2.64×10^{18} molecules/cm². Also, this system has been used for evaluating deuterium retention in bulk-boronized graphites after plasma bombardment [1].

From these TDS data, the activation energy (E_d) for the desorption process can be estimated using the relation [2]:

$$(E_d/RT_m^2) = (v_d n \sigma^{n-1}/\beta) \exp(-E_d/RT_m) \quad (1)$$

where n is the order of the surface reaction, T is the peak temperature, v_d is the frequency factor, σ is the concentration of the gas, β is the temperature ramp rate.

As part of ITER-R&D effort, erosion-redeposition experiments have recently been conducted on high- Z materials such as tungsten. It is planned that the activation energy for the desorption of deuterium from selected high- Z materials is evaluated using eq.(1).

[1] Y.Hirooka et.al. Fusion Technol. 19(1991)2059.

[2] P.A.Redhead Vacuum 12 (1962) 203

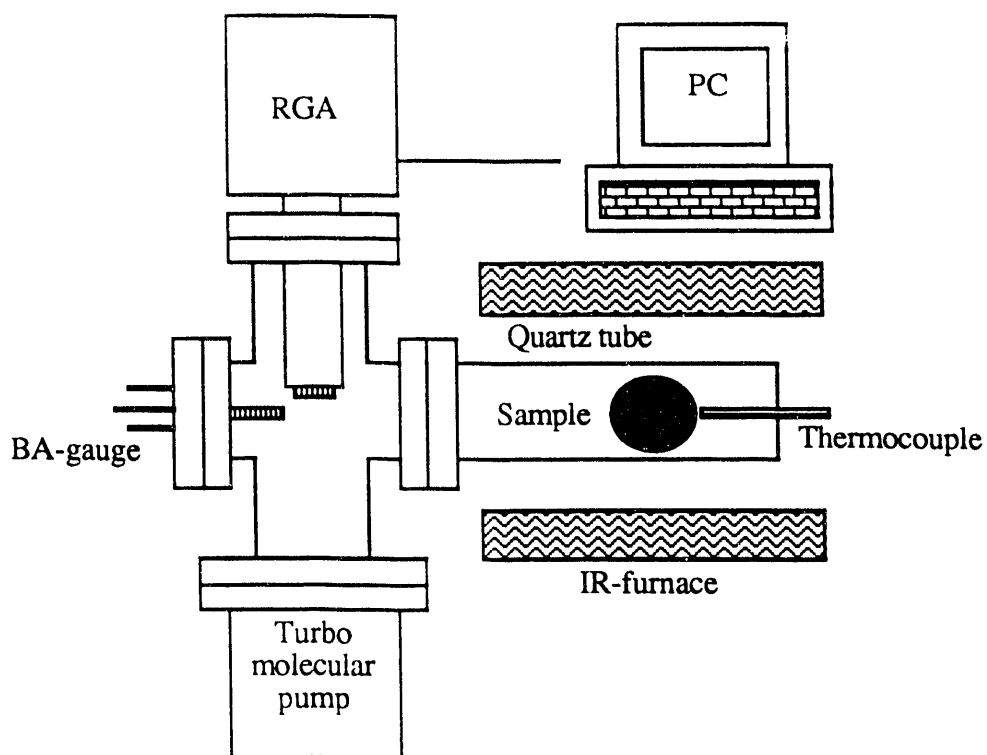


Fig. 1 A schematic diagram of the vacuum outgassing facility.

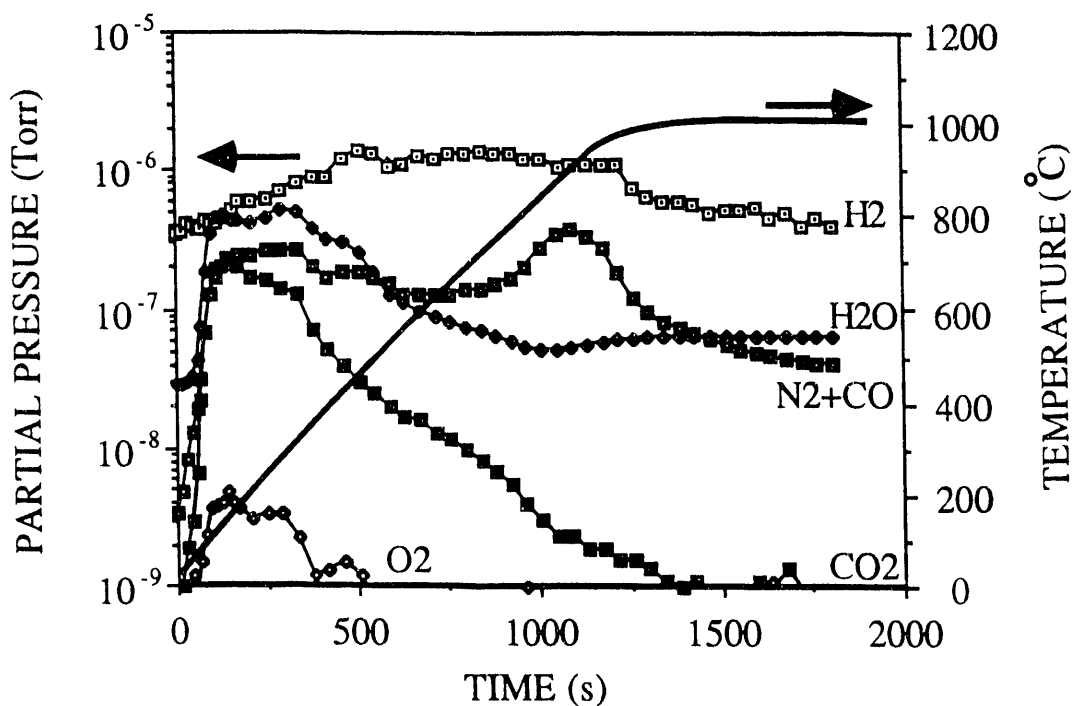


Fig. 2 Desorption from titanized C-C composite (CCTK-420).

PISCES Computer Data Acquisition System

The PISCES Data Acquisition System allows data acquisition, storage and manipulation of data from the PISCES-A, PISCES-B, PISCES-Jr and CCT Tokamak. The main components of this PISCES Data Acquisition system are the CAMAC(Computer Automated Measurement and Control) crates containing fast and slow data loggers which are connected to a VAX cluster, consisting of two VAX 4000, one DEC 3100/76 two Micro Vax-II and three VAX 2000 workstations. A Serial Highway Driver is attached to the Micro Vax-II which establishes the communication with CAMAC crates through the Fiber Optics cables, providing high voltage isolation from PISCES and CCT machines.

The CAMAC crate connected to the PISCES-A machines contains two 32-channel slow loggers and is capable of sampling data at a rate of DC up to 100 KHZ. The number of active inputs is programmable. To achieve maximum sampling rate fewer inputs are used depending upon the available memory in the crates. Individual channels have descriptive logical names assigned to them which facilitates user access to the raw and processed data. ORNL CAMAC crates drivers are used for setting up the data loggers and acquisition of the raw data from the CAMAC crates.

Recently the HYTEC Ethernet CAMAC module was successfully tested in PISCES facilities. The significance of this new CAMAC module is that it eliminates the need for CAMAC Serial Highway and with this ETHERNET controller the acquisition of data is done in the CAMAC and then the data is transmitted via the ETHERNET to the target Workstations. These Ethernet controllers are network devices which request on line load image from their workstation hosts. and software driver is loaded via the Ethernet. The data acquisition is done on the CAMAC bus and then the data is transmitted from memory modules to the intended target node in the cluster. On line load image through the workstation host will not be limited only to one node in the cluster. Several boot nodes in the PISCES cluster will have this network on line load capabilities which in turn removes the single point failure for the Data Acquisition system. The PISCES group is planning to upgrade all the CAMAC crates with the HYTEC controller during 1993 fiscal year.

The VMS operating system has been upgraded to 5.4 and in this upgrade all graphics window system and the users interfaces also upgraded to X-window system (DEC-windows). PISCES group developed the prototype graphics interfaces in this X-Window system so the workstations could become functional for the research staff. PISCES group also enhanced and upgraded the DACP(Data Acquisition control programs) so they can become operational in this new DecWindow environment. DACP controls the continuous as well as post-triggered data sampling on PISCES-A and PISCES-B

machines. The DACPs provide the users controlled data acquisition functions and also compute the processed data from the recently retrieved raw data. The CAMAC crate used by the CCT Tokamak contains two fast loggers each with 4 channels capable of sampling data at 1 MHz and one slow logger with 32 channels.

The MIT MDS software provides the database facilities for the VAX cluster environment which enables the structured storage of raw, processed and compressed data. Apart from this, other customized software using IDL, PVI-DI and DISSPLA graphics packages provide the realtime data analysis and manipulation capability. In addition PISCES group developed the double probe analysis code for analyzing the data from PISCESB .

Further improvements and refinements have been included in this software so it can be used at other sites. New data analysis applications have been developed based on the MOTIF graphics interface which gives event driven capabilities to the operation of the analysis software. This event driven capabilities permit the user to run the code both in the Batch mode or interactive mode. The events specified by the user determines the sequence of the analysis and this provides more friendly interface for the end user.

The PISCES group plans to be equipped with the high end INFO-SERVER 150 which provides additional X-access capabilities to the VAX cluster. The INFO-SERVER is a general purpose disk storage server that quickly and efficiently transfers data between disks connected to the server and remote network client systems . The INFO-SERVER functions includes : sharing software system, efficient data distribution without engaging another network node and booting media in the network.

The PISCES group within the next two fiscal year will provide a combination of high performance Workstations with INFO-SERVER so the VAX cluster will have the optimal CPU power and the X-access required for all the users. The VAX cluster is connected through the ETHERNET to several DecServer200 terminal servers connecting other varieties of peripherals(4 Macintoshes, 2 IBM PC/AT XT, TEK-4015, TEK 4696 for color graphics capabilities, modems for communications, and DEC Laser printer for hard copies). Terminal emulation programs executing on the Macintoshes and IBM PC facilitate transfer of data to and from the VAX Cluster environment to the remote PC systems.

The PISCES group has also acquired two 5000/200 DECstations running under ULTRIX 4.2 which will be used primarily for CAD/CAM applications. The state of art PRO-ENGINEER software with powerful 3-D graphics and visualization capabilities has been licensed for both workstations and are currently used by the Mechanical Engineering staff. The performance of the DECstations are enhanced with Turbo Graphics Accelerators which provide high speed graphics emulation as well as realtime computation.

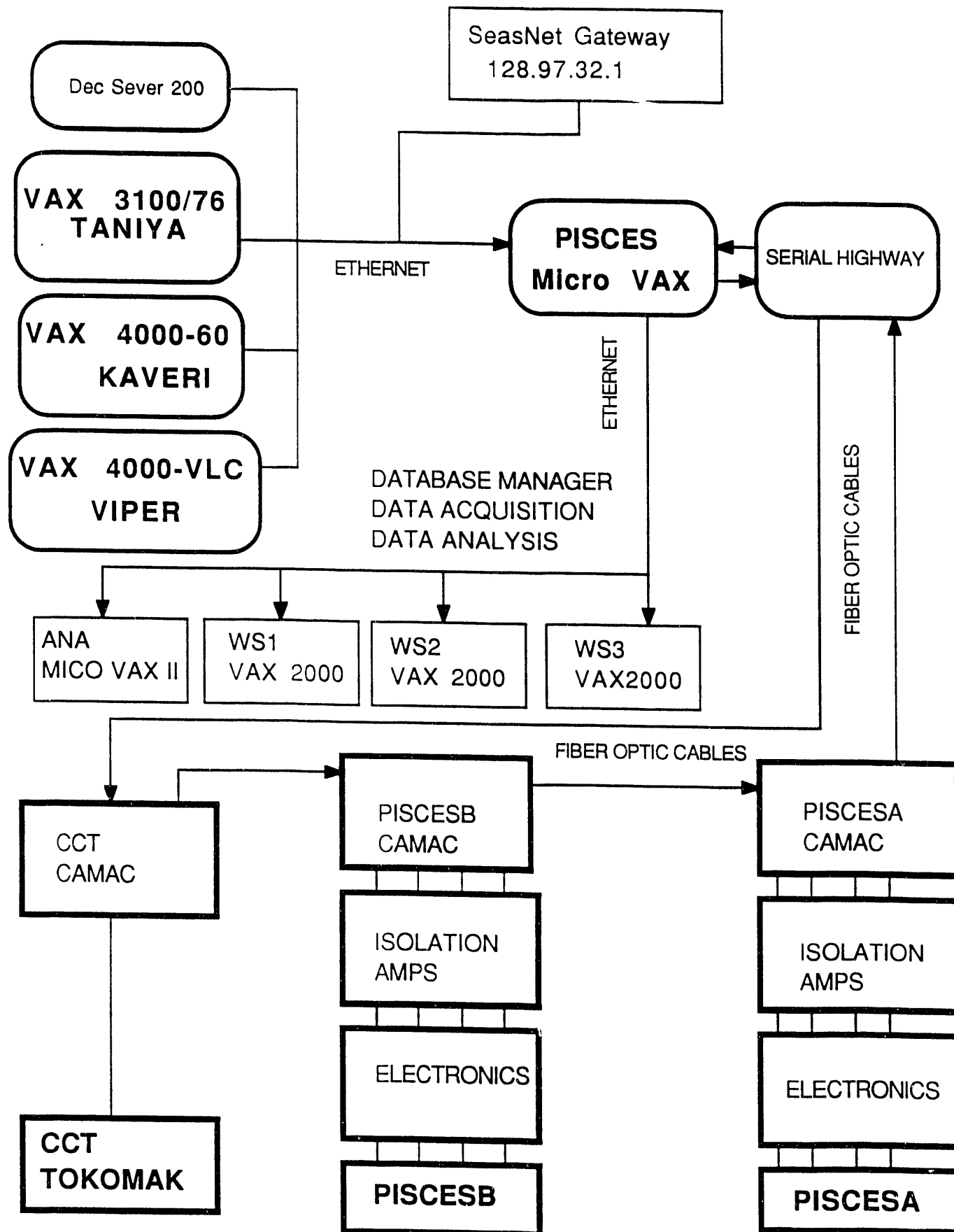


Fig .1 A schematic of the PISCES data acquisition system

3. PISCES Experiments

- Materials and Surface Physics -

Evaluation of Tungsten as a Plasma-Facing Material for ITER [1]

As part of the ITER-R&D effort at UCLA, tungsten in the form of bulk-material, relatively thick (1 mm) chemically deposited (CVD), and low-pressure plasma-sprayed (LPPS) coatings on molybdenum has been evaluated as a plasma-facing material, focusing on issues related to the divertor plate design. These issues are: (1) thermal outgassing; (2) plasma erosion; (3) deuterium retention; (4) disruption erosion. This work has been led by UCLA and conducted in collaboration with SNLL, ANL, NCSU.

(1) Thermal outgassing: Total outgassing quantities up to 1000°C from tungsten materials have been found to be of the order of 10^{17-18} molecules/cm², as shown in Fig. 1, orders of magnitude smaller than those from typical graphites including C-C composites. Among the tungsten materials tested, LPPS coatings tend to have higher outgassing rates. This is presumably due to the porous structure, necessitating R&D for higher density coatings.

(2) Plasma erosion: Deuterium plasma net erosion rates at 1500°C are basically the same for bulk tungsten, CVD and LPPS coatings. Generally, at ion bombarding energies below 400 eV oxygen-containing impurities (such as H₂O⁺) in the deuterium plasma dominate the total erosion rate of tungsten. The erosion data are shown in Fig. 2. On the other hand, it has been observed that at electron temperatures around 5 eV or lower, positive ionization of these impurities is significantly reduced, whereby plasma erosion data basically agree with sputtering theories and ion beam data. In fact, for oxygen the electron attachment reaction: $O_2 + e \Rightarrow O_2^-$ is dominant at electron temperatures below 10 eV.

(3) Hydrogen retention: Postbombardment thermal desorption measurements have indicated the deuterium retention quantity in tungsten materials is of the order of 10^{14-15} D-atoms/cm², which is considerably smaller than the corresponding data for graphites and C-C composites. Also, it is important to note here that there is no codeposition-driven tritium inventory with tungsten.

(4) Disruption simulation: Disruption-simulated high heat loads up to 6MJ/m² have caused microcracks in tungsten materials. As shown in Fig. 3, a strong heat shielding effect has been observed, decreasing the heat transmission factor to about 1%. This is explained by a molten layer protection effect, presumably combined with a mild vapor shielding effect.

Clearly, further effort is needed to improve the fusion-related quality of tungsten coatings. Because of its high probability of redeposition, in general tungsten neither causes heavy core contamination nor suffers from severe erosion even with an open divertor configuration. Nonetheless, the application of tungsten will be more viable if a gas target divertor configuration is implemented.

[1] Y.Hirooka et al., to be published in J.Nucl.Mater. (presented at 10th PSI conf.)

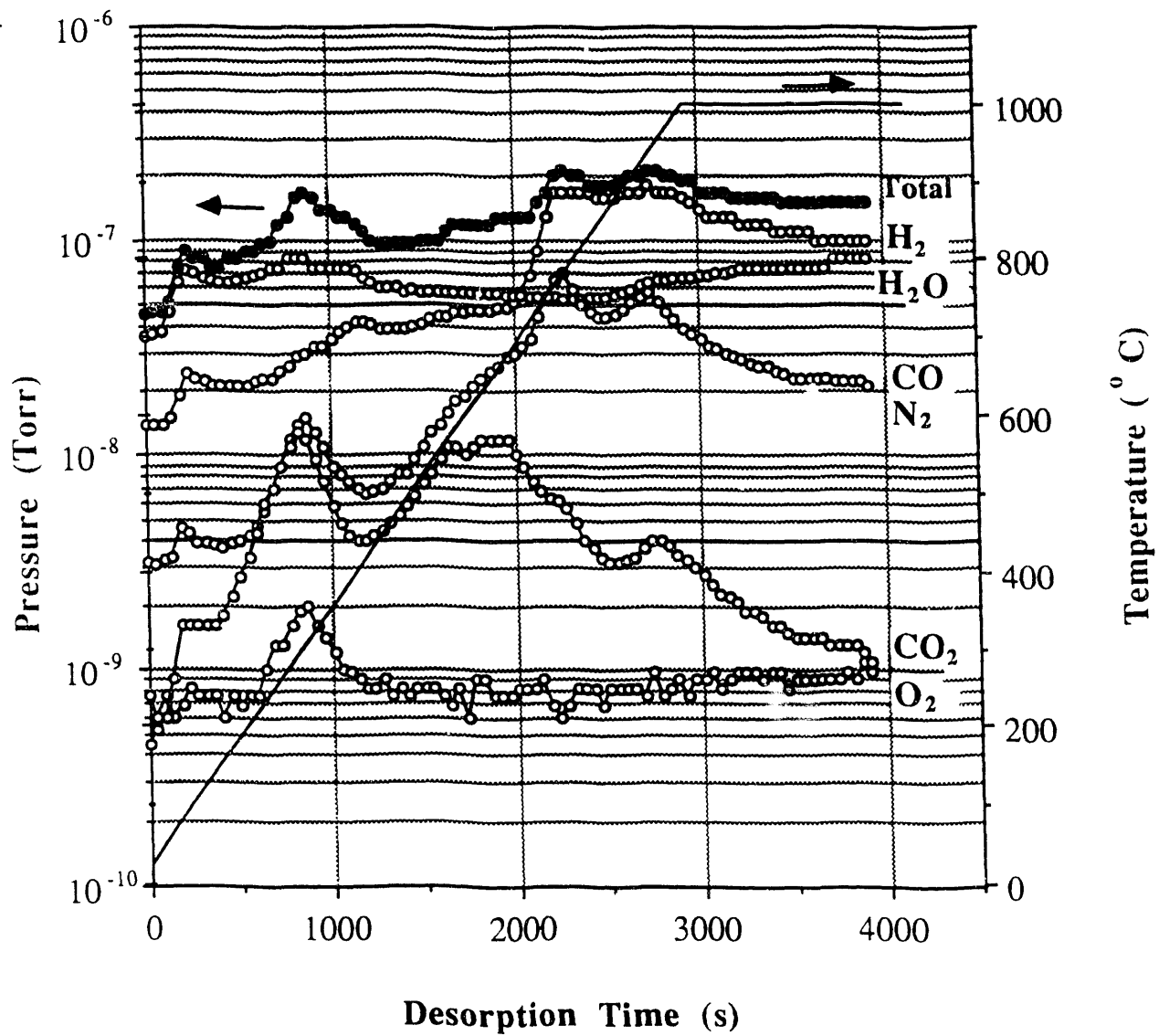


Fig. 1 Thermal outgassing from as-received bulk tungsten.

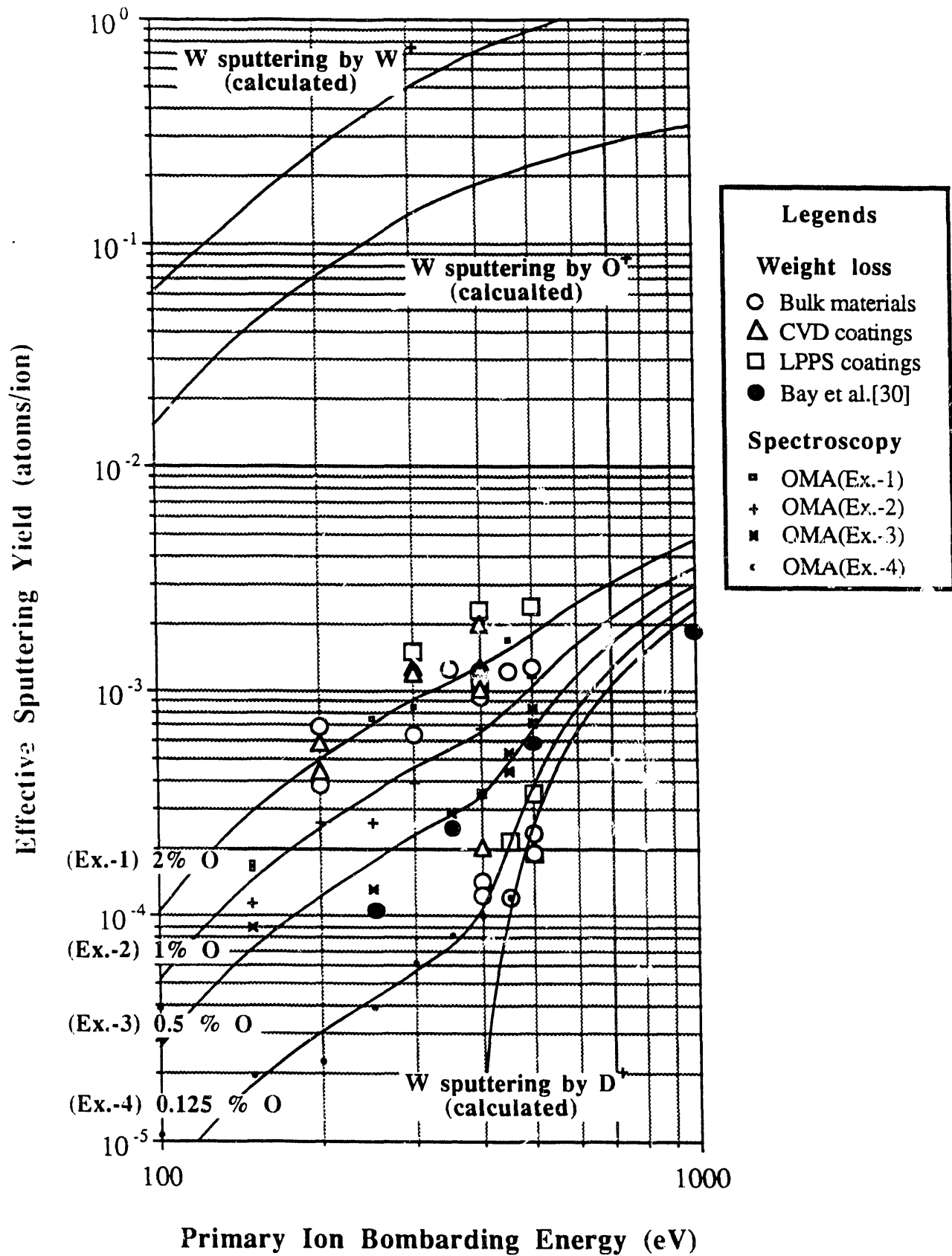


Fig. 2 Erosion of tungsten by O-contaminated D-plasmas.

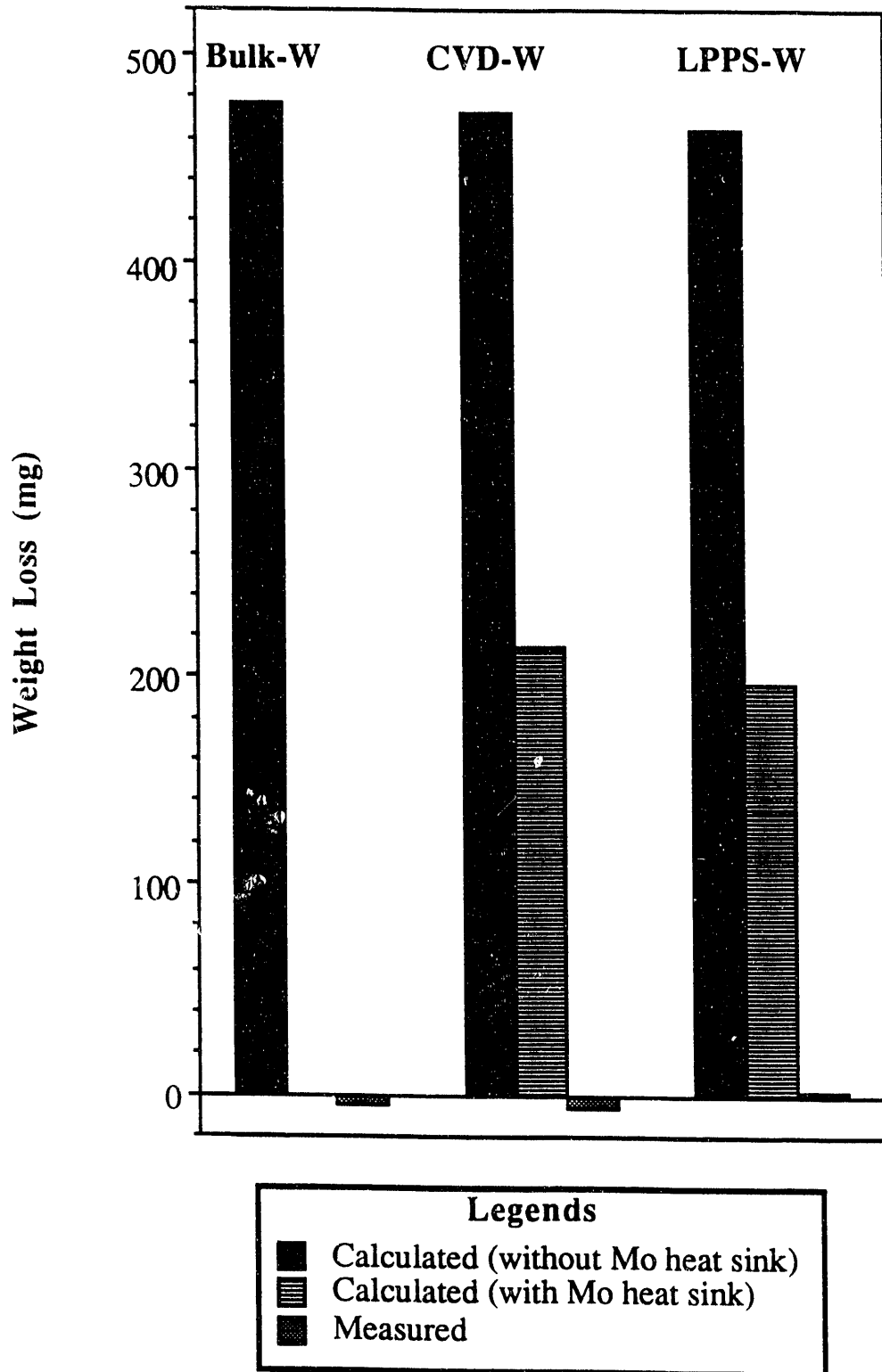


Fig. 3 Measured and calculated weight losses for tungsten materials tested in SIRENS at a disruption load of 6 MW/sq-m.

High-Flux Plasma Exposure Tests on Actively-Cooled Divertor Mock-up

It is widely recognized that to handle long-pulse and high-heat fluxes such as those to be seen at the ITER divertor plate, actively-cooled systems are absolute requirements in which either water or helium is used as the coolant. Because of their high availability, electron beams have been used as the high heat flux source in most high heat flux experiments. However, for the same heat load the material behavior under electron beam bombardment can be completely different from that under plasma bombardment. Critical differences are: (1) energy reflection and deposition depth; and (2) surface erosion. Obviously, there is a need for the data with plasmas used as the heat source. The present work is done as part of the US-Japan collaboration and is intended to provide the first data on the durability of water-cooled divertor mock-up units brazed with graphites under exposure to steady state and high-heat flux plasmas.

Shown in Fig. 1 is a water-cooled divertor mock-up assembly prepared jointly with JAERI on which four graphite samples are mounted, each with a plasma-facing area of about 1 cm^2 : (1) ultra-high thermal conductivity 1-D C-C composite (MFC-1: Mitsubishi Kasei); (2) isotropic graphite (IG430U: Toyo Tanso); (3) high-density C-C composite (CX2002U: Toyo Tanso); and (4) calorimeter made of IG430U (Toyo Tanso). Except the calorimeter, all samples were brazed on molybdenum blocks, which is again brazed on the water-cooled copper or stainless steel pipes. Also, samples #1 and #2 are on a stainless steel pipe whereas samples #3 and the calorimeter are on a copper pipe. This setup allows us to raise the surface temperature to the range relevant to ITER, even for ultra-high thermal conductivity C-C composites. These samples are attached with thermocouples so that temperature data can be monitored on-line during plasma exposure.

These samples were bombarded with high-flux deuterium plasmas in PISCES-B Mod as shown in Fig. 2. The maximum flux was 2.9×10^{19} ions/cm²/s, which is essentially the same as the peak ion flux expected at the divertor plate in ITER, 4×10^{19} ions/cm²/s [1]. Also, the effective deuterium ion bombarding energy was about 50-60 eV. Therefore, the heat flux associated with plasma ion bombardment is about 250 W/cm^2 (2.5 MWm^2). The water flow rate was controlled at about 9-10 liter/min. Under these conditions the surface temperatures measured with an optical pyrometer were: 800, 1340 and 550°C, respectively, for samples #1, 2, and 3.

Due to the high thermal conductivity, the 1-D C-C composite was found to remain in the temperature range of chemical sputtering whereas the isotropic graphite was heated to radiation enhanced sublimation. Also, from these findings one realizes that the effect of heat sink materials selection on the plasma-facing surface temperature is rather significant. Detailed energy balance analysis is under way.

[1] T.Kuroda et al., "ITER Plasma Facing Components", ITER Documentation Series #30, IAEA, Vienna

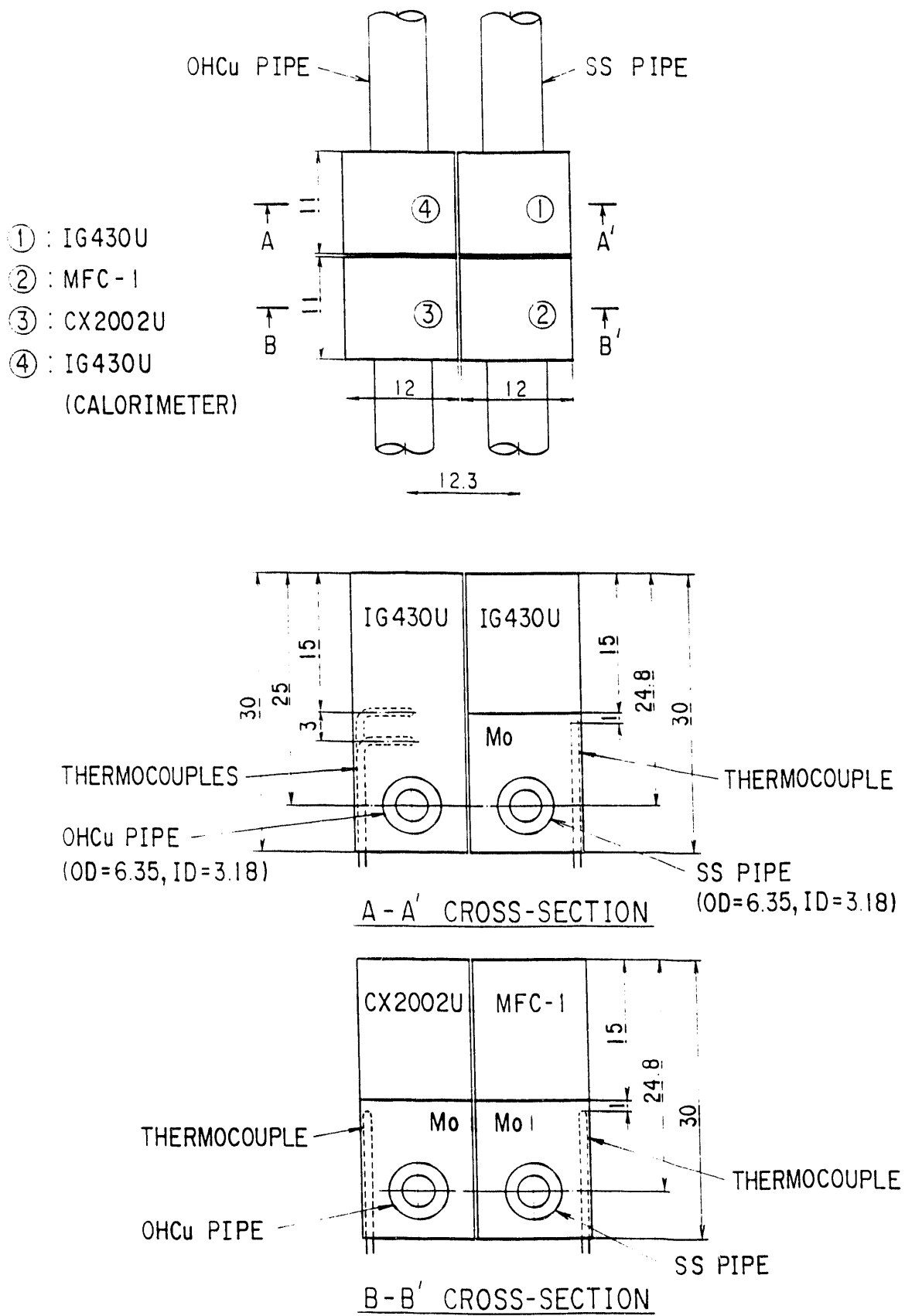


Fig. 1 Water-cooled divertor mockup brazed with various graphites.

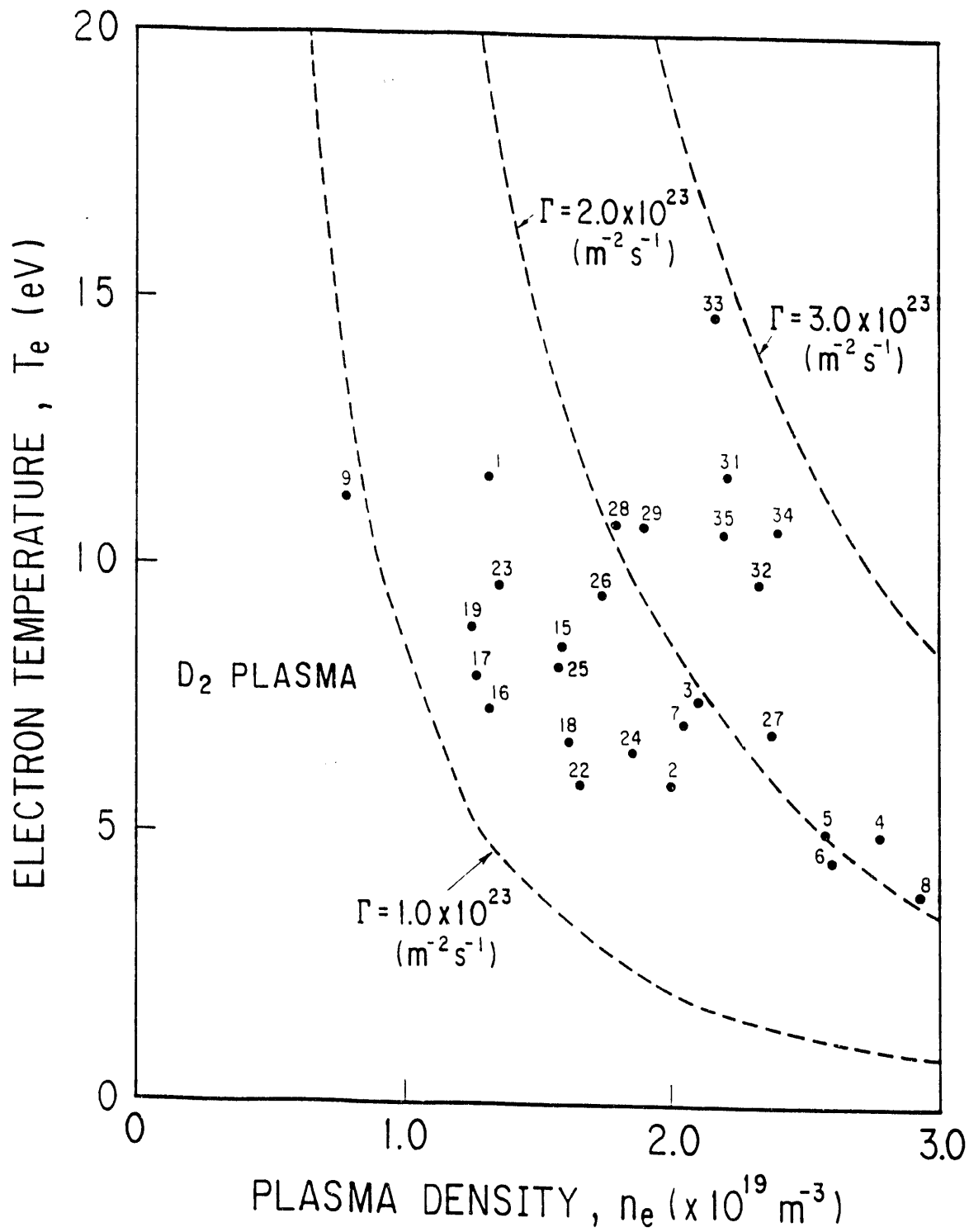


Fig. 2 Plasma densities and electron temperatures employed in the present experiment.

Impurity Transport under Steady-state Magnetized Plasma Bombardment

In magnetic fusion devices, materials eroded from surface components can be ionized due to electron impact, trapped by the magnetic field and then redeposited elsewhere. Therefore, redeposition may lead to a cross-field impurity transport. These erosion and redeposition effects directly affect the lifetime of plasma-facing components and influence the plasma cleanliness. In this work PISCES-B Mod. is used to conduct experiments to understand the impurity transport behavior under redeposition conditions.

Fig. 1 shows a schematic diagram of the experimental setup used for the experiments. A graphite target plate, with a boron or molybdenum "impurity" marker embedded at its center, is exposed to a steady state argon plasma. In this preliminary work, the magnetic field is set at 500 G at normal incidence to the substrate surface. The plasma density is maintained at about $2 \times 10^{12} \text{ cm}^{-3}$ and the electron temperature at about $18 \text{ eV} \pm 2 \text{ eV}$. The ion bombarding flux is about $1 \times 10^{18} \text{ ions/cm}^2/\text{s}$ and the ion bombarding energy is controlled in the range from 100 to 150 eV by applying a negative dc-bias on the graphite substrate. Boron and molybdenum are used as the impurities. Under these plasma conditions, the redeposition fraction of these materials has been calculated to be from 30 to 45%, using the WBC code [1].

After plasma exposure for duration ranging from 0.5 to 60 minutes, surface analysis with EDX is performed to determine the impurity concentration profile. As shown in Fig. 2 we see that the impurity concentration shows a general tendency to decrease exponentially from center towards the edge. At each radial position (see Fig. 3), the impurity concentration tends to saturate after a certain plasma fluence. SEM analysis indicates no significant change in surface morphology. Surface segregation of carbon, forming an overlayer on the marker, can reduce the erosion rate [2]. At present the cause for the saturation behavior is not yet clearly understood. Nonetheless, this behavior has been fitted by the relation: $C = C_{\text{max}}[1 - \exp(-t / \tau)]$, where C is the impurity concentration, τ is the characteristic time constant and t is the plasma exposure time. Value of τ are plotted in Fig. 4 as a function of position. It is found that generally, transport of boron (low-Z) material is more rapid than that of molybdenum (high-Z) material. Also, the increase in ion bombarding energy results in a decrease in τ , indicating that the sputtering yield plays an important role in determining the effective transport rate.

Currently, we are conducting similar impurity transport experiments with a non-normal incidence of the magnetic field, intended to be more relevant to plasma-surface interactions conditions in fusion devices.

[1] J. N. Brooks, Phys. Fluids. B 2(8) (1990) 1858.

[2] K. Morita, Fusion technol. 19(1991)2083.

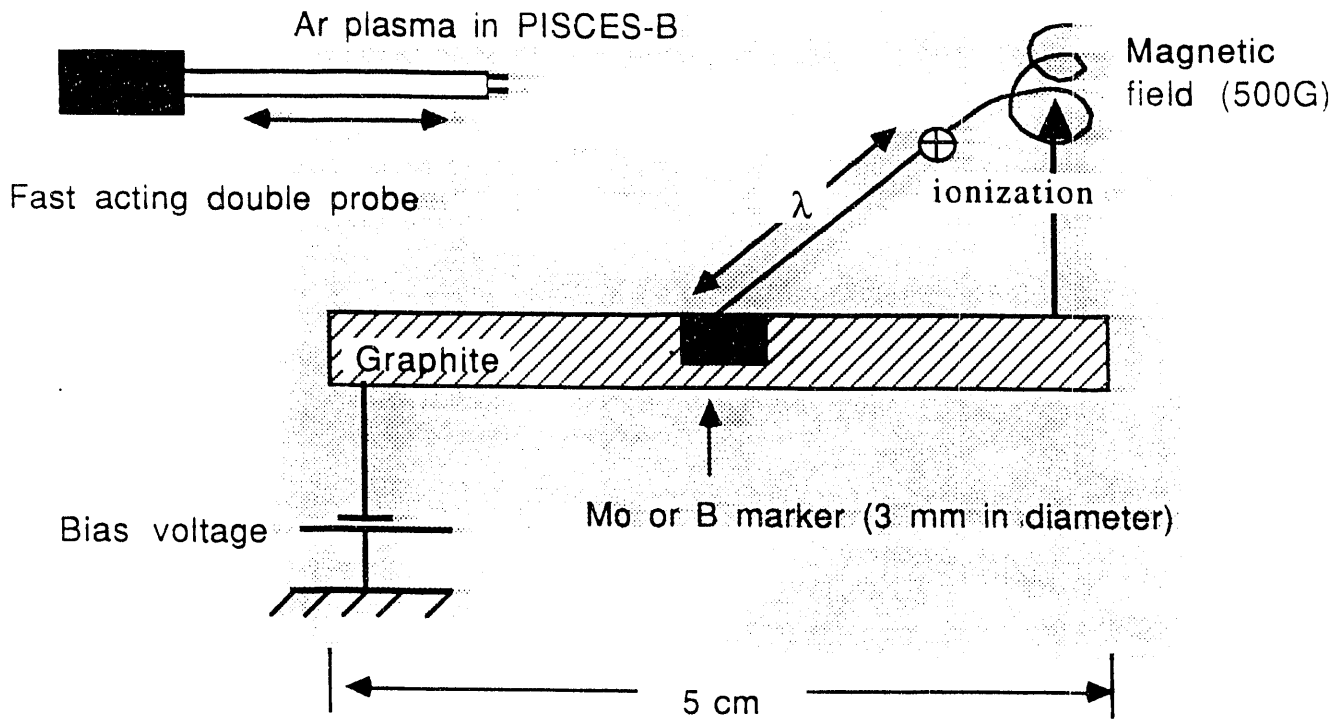


Fig. 1: A schematic diagram of the experimental setup

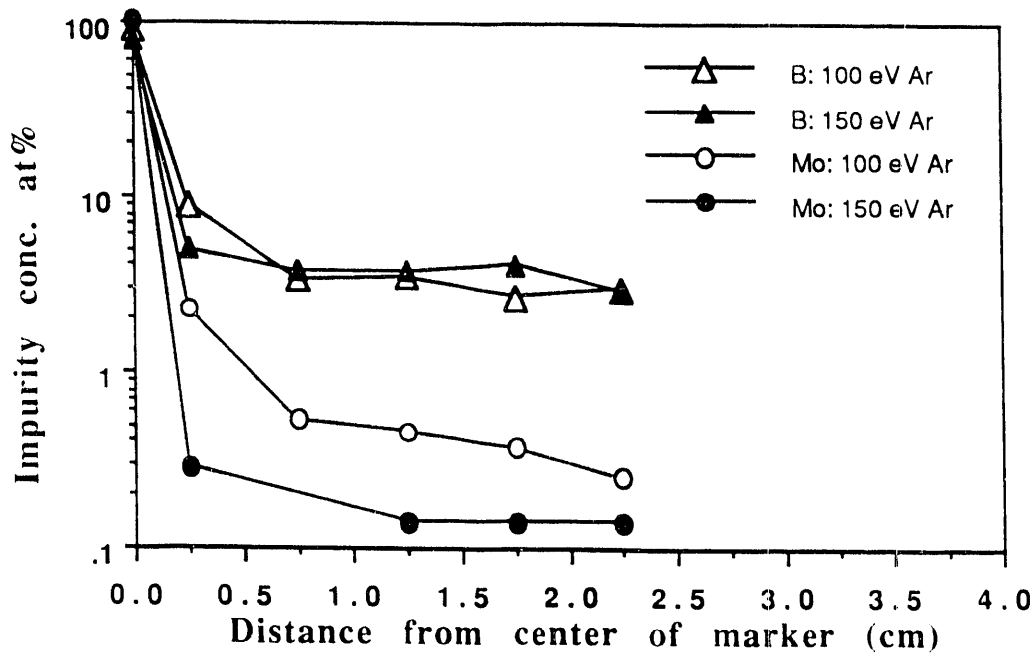


Fig 2: Radial concentration profile obtained by EDX analysis after 60 min. plasma exposure

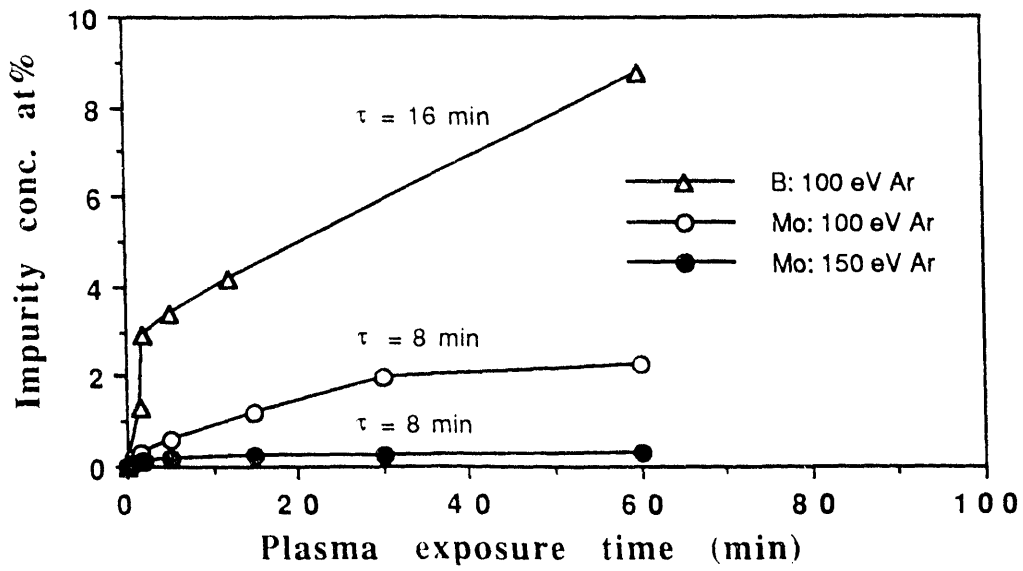


Fig 3: Time dependence of impurity concentration on the graphite surface at the position closest to the marker

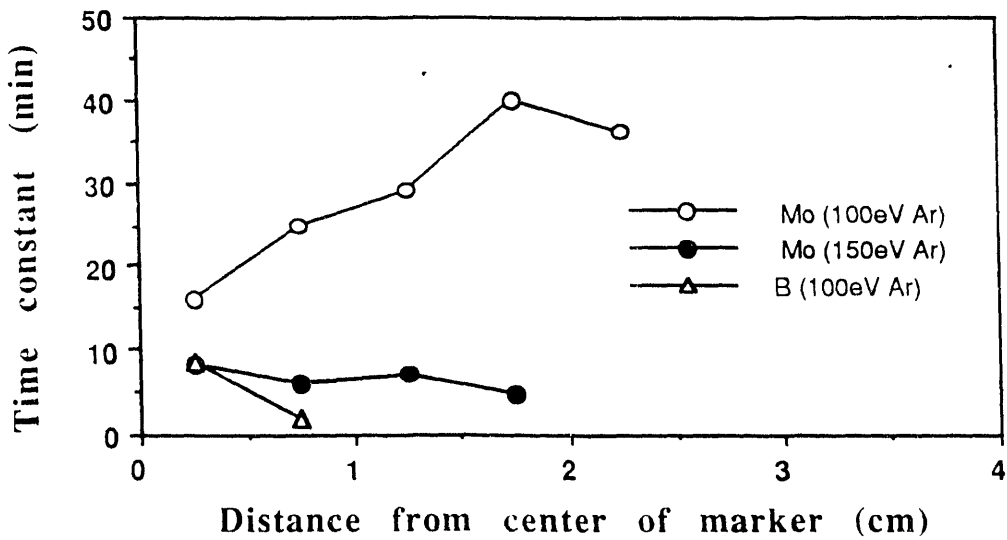


Fig 4: Dependence of the characteristic time constant on the distance from the marker.

Surface Topographical Modifications due to Erosion and Redeposition *

As predicted by theories [1,2], high-fluence plasma bombardment can lead to microscopic as well as macroscopic surface topographical modifications on plasma-facing components if redeposition is not uniform. It is also true that these surface modifications accelerate or decelerate the erosion process in a yet-to-be explored manner because in general the sputtering yield is a function of incident angle. However, there has been little information on this subject except long-term exposure data from tokamaks. Unfortunately, the data from existing tokamaks are difficult to interpret because the plasma exposure is not done at the steady state and disruptions also affect wall erosion significantly.

In this experiment, using the PISCES-B facility, steady-state plasma exposure experiments have been conducted for graphite samples (IG-430U, Toyo Tanso) with a surface smoothness controlled within about $\pm 1 \mu\text{m}$ across the diameter of 5 cm. Hydrogen and helium plasmas are used to investigate two different cases: (1) a relatively short ionization mean free path for ionization for hydrocarbons due to chemical sputtering (2) a long mean free path for physically sputtered carbon. The plasma density profile measured by a fast scanning probe is found to have a FWHM of about 5 cm. The target surface temperature (at the center) is measured with an infrared pyrometer.

Shown in Fig. 1 are the surface profiles after extended exposure to a helium plasma at 100 eV and a hydrogen plasma at 70 eV to the total fluence of the order of 10^{22} ions/cm². The mean free path for carbon and methane are about 10 cm and 1 cm. From these conditions little redeposition is expected for carbon whereas the opposite is true for methane. Consistent with this, the He-bombarded surface profile shows an erosion-induced crater with a depth of about 120 μm . Also, the erosion yield calculated from the weight loss measurement agrees with that estimated from the volumetric loss due to the formation of the erosion crater. On the other hand, the H-bombarded surface indicates materials redeposition, a convex profile, although it is difficult to define the reference topography. As shown in Fig. 2, the surface microstructures observed at the edge shows a typical eroded surface morphology whereas interestingly in the convex region one finds a sign of columnar growth. One possible cause for this convex profile is as follows. Although the measured temperature at the sample center is 950°C, perhaps the edge temperature may be lower due to the plasma density profile. Therefore, methane generated at the edge due to chemical sputtering is redeposited at the center where only physical sputtering is presumed. A detailed analysis is under way.

*Experiment conducted jointly with NIFS as part of the US-Japan collaboration.

[1] J.N.Brooks, Fusion Technol. 18(1990)239.

[2] A.Sagara et al., to be published in J.Nucl.Mater. (presented at 10th PSI conf. 1992).

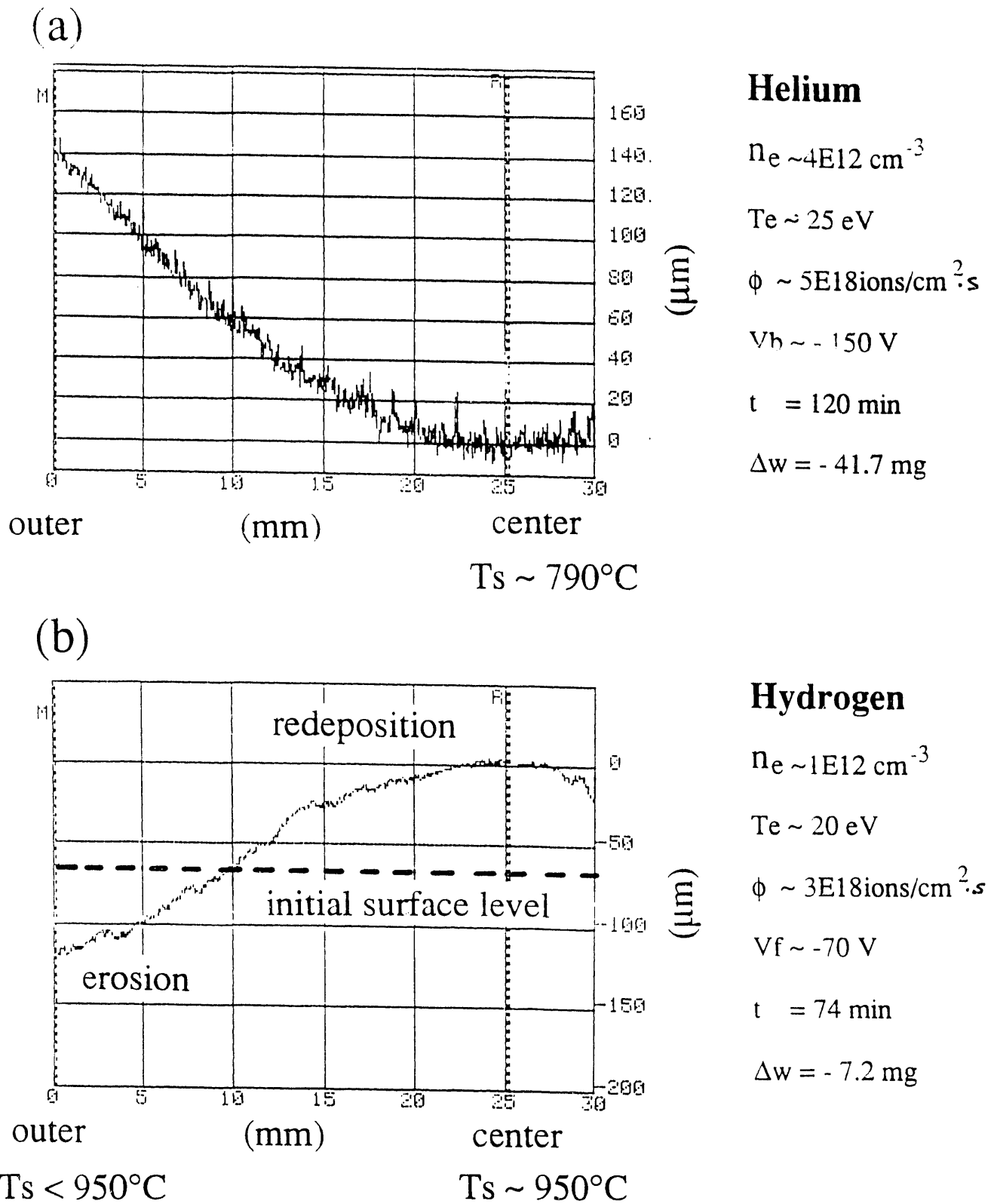
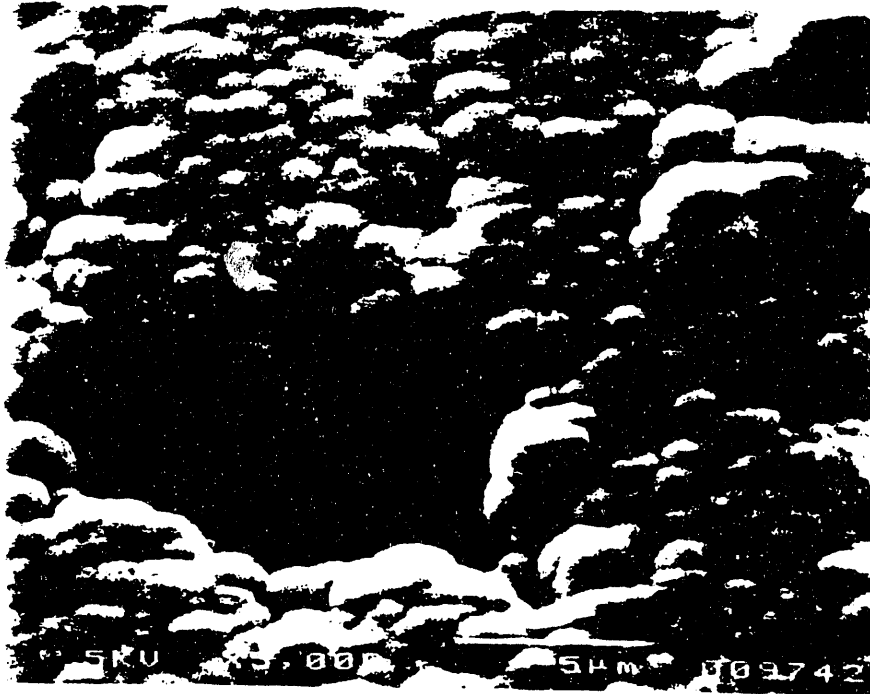


Fig.1 Surface profilometry of graphite samples eroded with (a) helium or (b) hydrogen plasma.

(a) center region



10 μm

(b) outer region



Fig. 2 SEM photos taken at the (a) center and (b) outer region of the graphite sample bombarded with H plasma.

4. PISCES Experiments

- Edge Plasma Physics -

Heat Flux Reduction and Impurity Screening in a Gas Target Divertor

-Simulation Experiments in PISCES-A-

Management of the divertor heat-load deposition is a critical issue for the design of next generation fusion devices such as ITER. The heat load to the outer divertor region is estimated to reach values of up to 50 MW/cm² in ITER during the technology phase. The severe erosion and impurity control problems at these power levels have stimulated research on alternative divertor concepts. The idea of the reentrant divertor is to redistribute the divertor heat flux over a large surface area by radiation and/or elastic and inelastic collisions with neutral particles. A wide range of experiments has been performed in PISCES-A to simulate a divertor plasma interacting with a neutral gas target and to evaluate the relevant atomic physics and plasma transport processes [1]. Recent experiments have focused on obtaining a high density hydrogen plasma with electron temperatures in excess of 15 eV, with the goal to produce ITER-relevant heat flux to the simulated divertor target.

The basic set-up of the gaseous divertor simulation experiment in PISCES is shown in Fig. 1. Downstream at a distance of about 1 m from the plasma source, the flowing plasma is accepted in a water-cooled circular neutralizer tube. The axial magnetic field can be varied from 0.04-0.19 T. The simulated divertor target is located at the downstream side of the tube ($z=0$). The tube is made of anodized aluminum and is electrically floating. Neutral gas (H_2 , D_2 , He, Ar) can be fed from the end of the divertor tube. The neutral pressure in the plasma source can be kept well below 1 mtorr even at high secondary gas feed rates. An axially moveable Langmuir probe provides measurements of the electron temperature, plasma density and floating potential profiles along the length of the divertor tube. The chamber neutral pressure is measured with an ionization gauge, and the neutral pressure at two axial positions inside the tube (at distances $z = 1.5$ cm and $z = 43$ cm from the divertor target) is recorded with ionization and baratron gauges. A CID camera as well as a 1.3 m Czerny Turner spectrometer with a photomultiplier tube is used to analyze plasma and neutral line radiation. A fast scanning, pneumatic Langmuir probe is used to obtain radial profiles of the plasma density and the space potential at select axial positions. A multitip radial probe is used to obtain the density and potential fluctuations \tilde{N} and $\tilde{\phi}$ as a function of plasma radius. The radial particle flux driven by fluctuating electric fields is evaluated from the probe signals.

Previous experiments with hydrogen and argon gas targets have shown that a neutral density of 10^{14} - 10^{15} cm⁻³ inside the plasma is necessary to access the "gas target" regime (where the electron temperature as well as the plasma density are decreasing towards the target).[1] At the high densities expected in the ITER divertor region ($n_e = 10^{14}$ - 10^{15} cm⁻³)

the neutral ionization mean free path is much smaller than the plasma diameter and the plasma is almost opaque to hydrogen neutrals (or injected impurity neutrals such as neon or argon). In turn, a fairly high gas pressure ($p_n < 1-10$ torr) is required at the plasma periphery in order to maintain the required no inside the plasma column.

We have demonstrated access to the gas target regime for plasma densities as high as $5 \times 10^{13} \text{ cm}^{-3}$ ($kT_e < 15 \text{ eV}$). Improved differential pumping in the plasma source as well as a particular plasma start-up sequence are critical to achieve these parameters. Typical axial profiles of the electron temperature, the plasma density and the neutral pressure P_n in the "neutralizer" regime are presented in Fig. 2. The magnetic field is 1.7 kG. Here, the hydrogen neutral pressure reaches 0.18 torr close to the target at the end of the neutralizer tube. For reference, the neutral pressure measured with the plasma shut off, P_{n0} , is also shown. The pressure increase (a factor of 2.7) is due to plasma pumping effects. The maximum heat flux measured upstream close to the tube entrance exceeds 4 MW/m^2 (corresponding to one quarter of the projected ITER divertor heat flux during the physics phase). The electron temperature is observed to decay from $kT_e = 18 \text{ eV}$ close to the tube entrance ($z = 90 \text{ cm}$, not shown) to $kT_e = 2 \text{ eV}$ at the divertor target. This corresponds to a heat flux reduction of 94 %. The plasma density presently achieved is limited by tolerable the heat load to the (water-cooled) probe diagnostics. We expect to be able to operate close to $n_e = 10^{14} \text{ cm}^{-3}$ if fast injection probes are used.

Impurity injection experiments have been carried out to evaluate the potential of the gas target divertor for impurity screening. This is important not only for intrinsic plasma impurities, but also, if impurity seeding is envisioned in order to increase the radiative energy loss in the divertor area (a lower hydrogen neutral density would be required in this case to control the divertor electron temperature). A trace amount of argon, neon or xenon has been injected through the target plate. The impurity neutral and ion density can be estimated from spectroscopic line intensity measurements at different positions along the neutralizer tube. Figs. 3 and 4 show the radially line-integrated impurity densities for Ar I and Ar II (determined from the Ar I line at 7504 \AA and the Ar II line at 4806 \AA), measured at $z = 43 \text{ cm}$, as a function of the neutral hydrogen density (averaged between $z=0$ and $z = 43 \text{ cm}$). The argon injection rate was kept constant. A dramatic reduction of the impurity concentrations with increasing hydrogen neutral density is observed, indicating effective impurity screening. Employing a fluid model (1 1/2-D), we find that the enhanced impurity screening is due to collisions between neutral argon atoms and directional hydrogen neutrals flowing towards the divertor target.

[1] L. Schmitz, et al., Journal of Nuclear Materials 176&177 (1990) 522

[2] L. Schmitz, et al., to be published in J.Nucl.Mater. (presented at 10th PSI conf.)

PISCES Gaseous Divertor Experiment

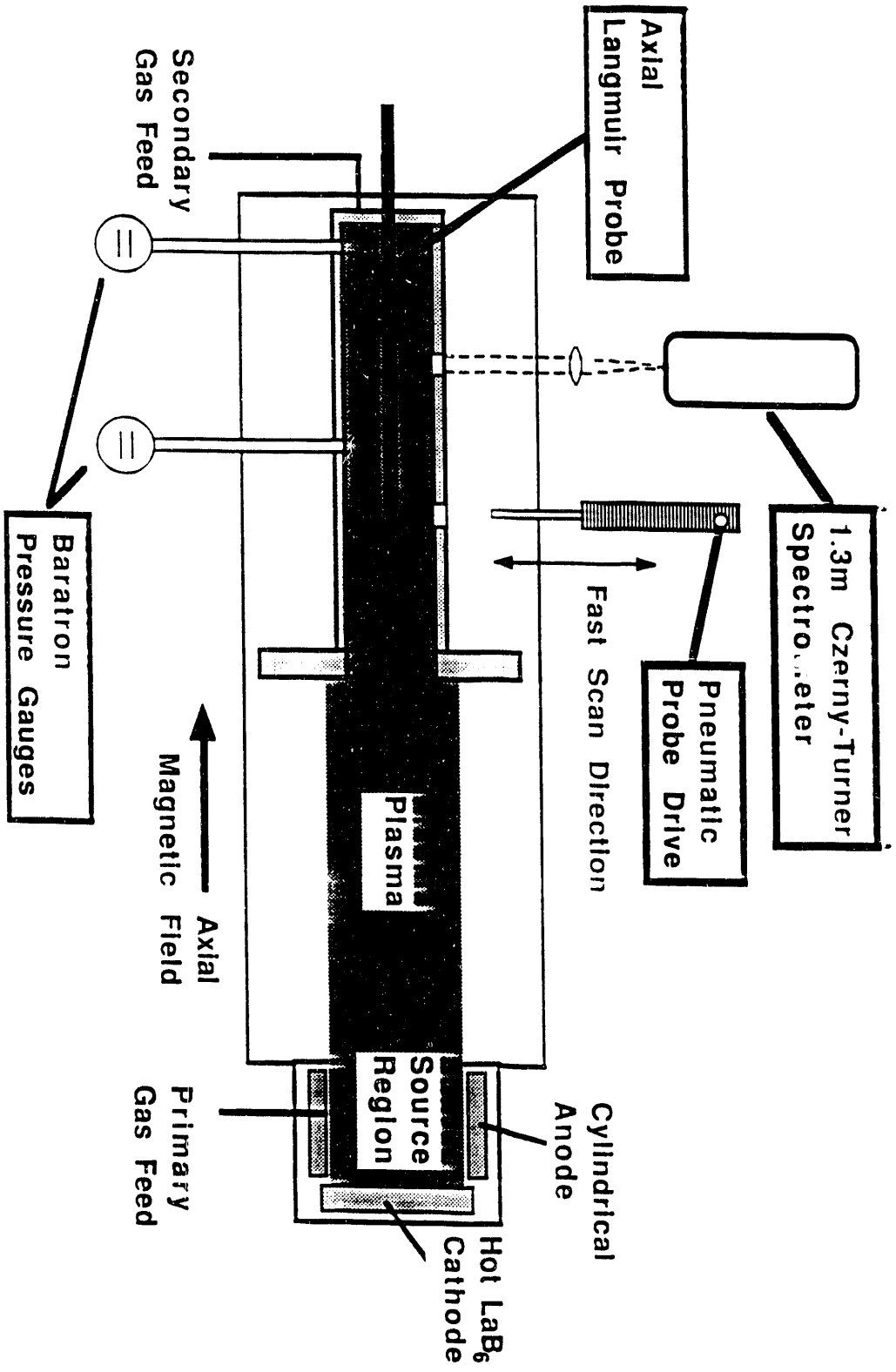


Fig. 1 Schematic of the experimental set-up for the gaseous divertor simulation in PISCES-A, showing the plasma source, the neutralizer tube and various diagnostics.

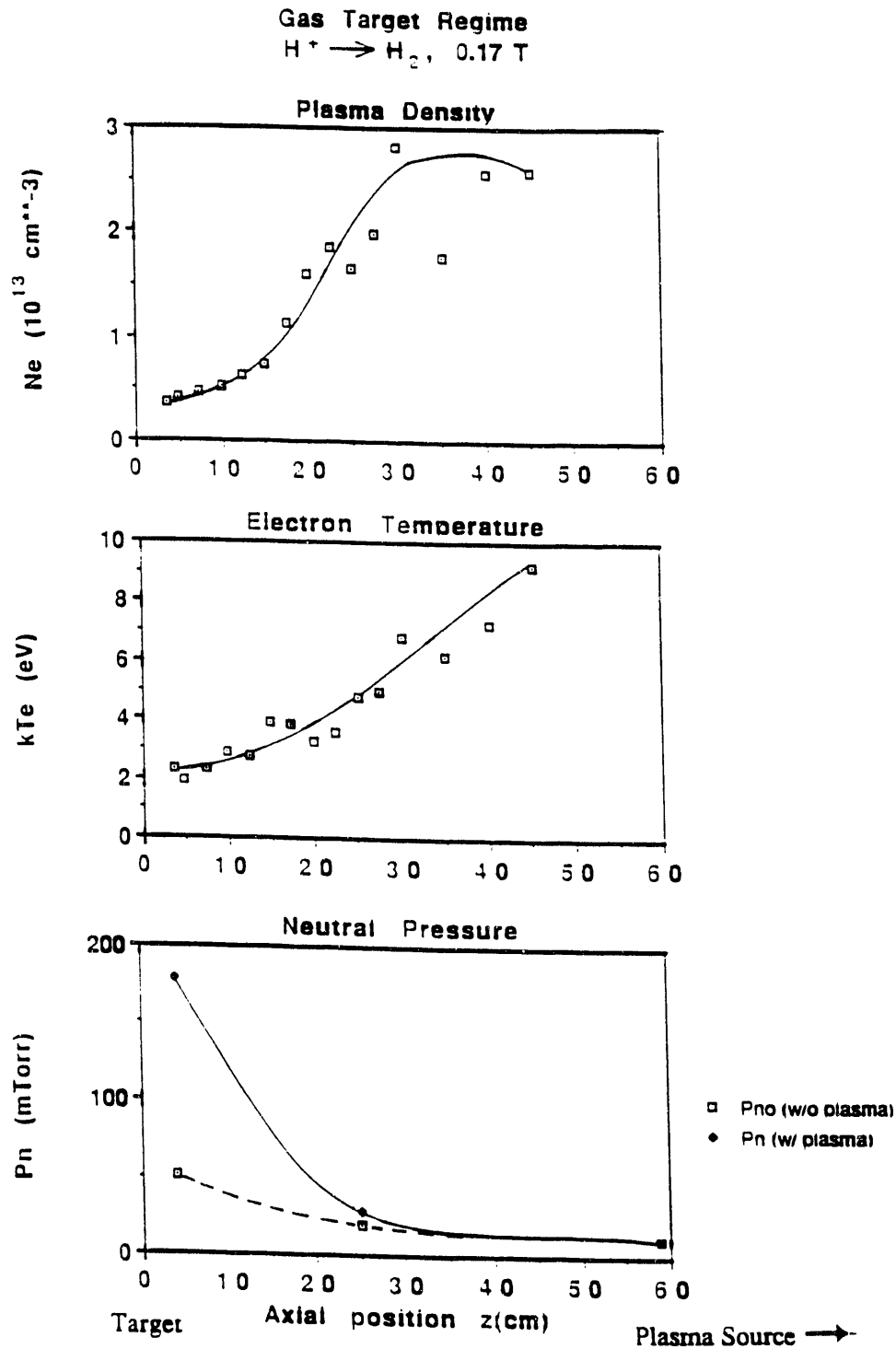


Fig. 2 Axial profiles of the plasma density, electron temperature, and neutral pressure in the gas target regime; a high density hydrogen plasma is injected from the right. The simulated divertor target is located at $z=0$; the neutralizer tube entrance is at $z=90$ cm (not shown).

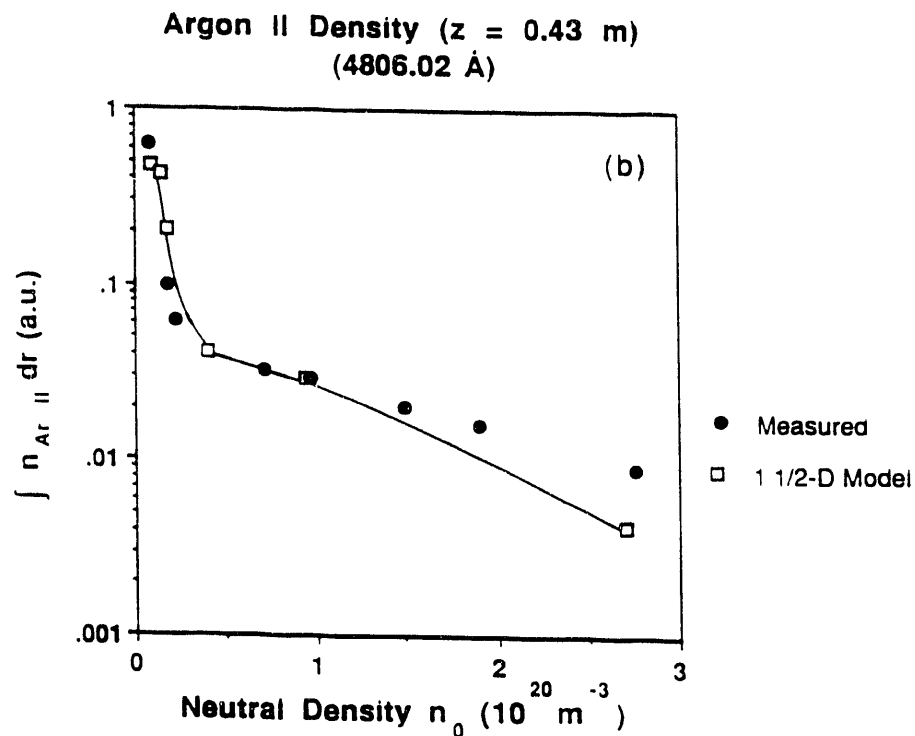
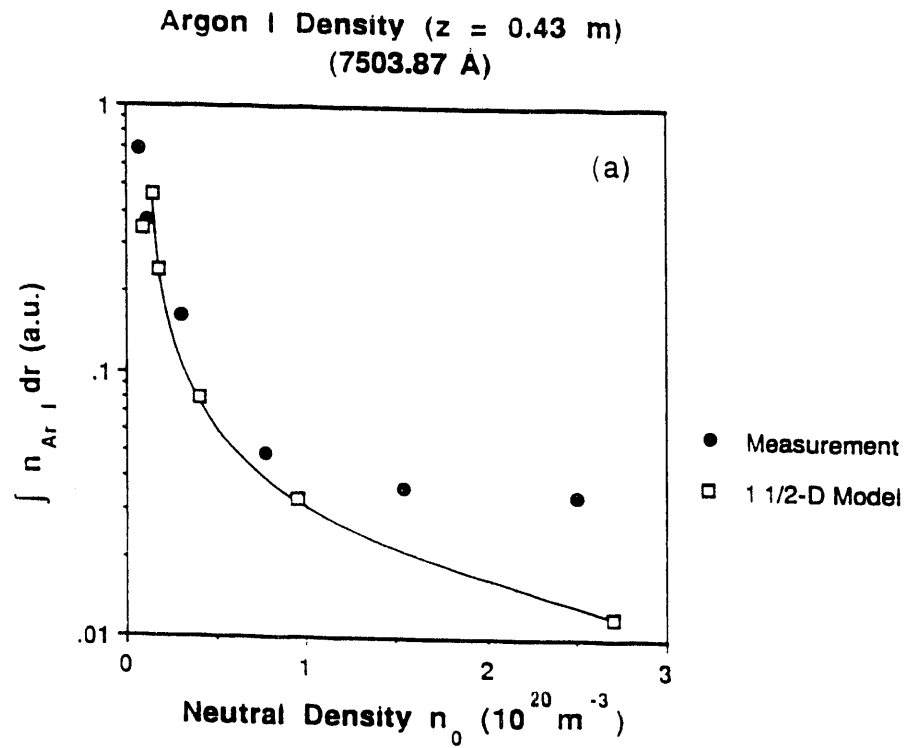


Fig. 3 a) Radially integrated argon neutral density, determined from of the Ar I line at 7504 Å, measured at $z = 43$ cm, as a function of the averaged neutral hydrogen density; b) Radially integrated argon ion density, determined from of the Ar II line at 4806 Å, measured at $z = 43$ cm, as a function of the averaged neutral hydrogen density.

Studies of heat transmission through the plasma sheath

A series of collaborative experiments between personnel from the PISCES Laboratory and personnel from Lawrence Livermore National Laboratory working on the DIII-D Tokamak at General Atomics have been initiated to examine heat transmission through the plasma sheath. These experiments are motivated by measurements of anomalously low values of the plasma sheath power transmission factor at the divertor plates in DIII-D. A theory has been developed which takes into account atomic collisional processes within the electrostatic sheath region [1]. This collisional theory predicts substantial reductions of the power transmission factor with increasing neutral density in the region of grazing magnetic field incidence at the wall.

PISCES-A has been modified to simulate the divertor region of a tokamak. A long dump plate has been constructed and inserted into the device at an angle of 5° with respect to the incident plasma column. A calorimeter is flush mounted in the face of the dump plate to measure the power incident on the surface. Standard Langmuir probes measure the plasma parameters directly in front of the plasma sheath and these values can be used as input to the collisional sheath model, as well as the collisionless models, to calculate the sheath power transmission factor. By varying the operating pressure in PISCES-A, a controlled investigation of the effect of neutral density in the sheath can be performed.

These measurements could have a major impact on the design of future large tokamaks where the issues of heat removal, sputtering and wall erosion are of the utmost concern.

[1] A. H. Futch, G. F. Matthews, D. Buchenauer, D. Hill and G. D. Porter, "Spatial Dependence of the Sheath Power Transmission Factor in DIII-D", General Atomics Report D3DPM No. 9103.

Edge Plasma Characterization in the CCT tokamak

The PISCES-CCT edge physics collaboration has continued during 1991. In this work, tokamak edge plasma transport physics are being studied using an extensive poloidal probe array (P²A) diagnostic that has been constructed and installed on the CCT tokamak (Fig. 1). The probe array can measure equilibrium plasma density, electron temperature and plasma potential as well as the edge plasma fluctuations. In this way, a comprehensive picture of edge plasma transport is being constructed.

A number of significant findings emerged from this work during 1991 and are listed below in an abbreviated form.

- Large-scale, large amplitude convective cells have been found inside the limiter radius, i.e. in the edge region of the plasma core. The maximum convective velocity is nearly one half of the local sound speed.
- An order-of-magnitude poloidal variation in the turbulent-driven particle transport exists. Nearly all of the transport occurs in the region characterized by magnetic field lines with 'bad-curvature'.
- Changes in the radial density decay length corresponding to variations in the cross-field particle fluxes are observed. Significant poloidal variations of plasma density and electron temperature are also found. Density and electron temperature vary by a factor of two at the last closed magnetic surface. These variations correspond to the poloidal distribution of radial particle transport.

Data illustrating the first point is shown in Fig. 2. Here, the P²A diagnostic has been used to measure the two-dimensional plasma potential distribution $\phi_{pl}(r,\theta)$. Large amplitude ($\Delta\phi \sim k_B T_e/e$) time-stationary plasma potential maxima are localized radially to the region around limiter radius ($r/a=1$). These potential maxima have a significant ($\Delta r/a \sim .1$) radial width (here a is the plasma minor radius) and are elongated in the poloidal direction (poloidal mode number $m \sim 4 - 5$). These structures are stationary in the laboratory frame. Their structure may change with a change in plasma current, toroidal magnetic field, and/or edge safety factor q_a . The resulting electric field has both radial and poloidal components and hence will include a particle drift of the edge plasma. Since the spatial scale of the potential distribution is much larger than the particle gyroradius, the potential contours then correspond to the $E \times B$ flow streamlines. The maximum flow speed is nearly half the local ion-acoustic speed.

These large scale convective patterns modulate the local microturbulence amplitude as well. The root-mean-square fluctuating poloidal electrical field amplitude is shown in Fig.3. The data indicate that the turbulent electric field fluctuations are largest at the interface between adjacent large-scale convective patterns. This suggests that the convective patterns are a driving source for the turbulent fluctuations. In this scenario, the large-scale convective patterns decay and generate small-scaled vortices which are damped as they propagate away from the excitation region. Additional analysis and measurements are needed to confirm this physical picture.

Large-scale convection is the dominant particle transport mechanism inside the limiter radius in CCT. At the limiter radius both turbulent particle transport and large scale convection are important transport processes. In the scrape-off layer, turbulent transport is the dominant particle transport mechanism. In CCT the total radial transport of particles varies significantly with poloidal position. Variations in the local density and electron temperature that correspond to the local radial transport rate are also observed.

These results indicate that flux-surface averaged pictures of transport present a limited view of tokamak transport. Additional measurements in CCT are needed to study the origin of the convective cells and to confirm the relationship between large scale convection and small scale plasma turbulence. Two-dimensional flow visualization techniques should be tried in CCT to make a direct observation of the convective patterns. A search for similar convective patterns in other tokamaks is also being planned and initial experiments will be performed on the TEXTOR tokamak during late 1991 and early 1992. If such patterns are found in TEXTOR, then large-scale convection may prove to be an important transport mechanism that exists in all tokamak devices.

Relevant publications

- [1] G.R. Tynan, "Two-dimensional particle transport in the CCT tokamak edge plasma UCLA-PPG-1369, June 1991.
- [2] G.R. Tynan et al. "Steady-state convection and fluctuation-driven particle transport in the H-mode transition" to be published in Phys. Rev. Lett.
- [3] G.R. Tynan et al. Bull. APS 36:9 2500(1991).
- [4] G.R. Tynan et al. Proc. on 18th Euro. Conf. on Controlled Fusion and Plasma Physics, June 1991 Berlin, FGR, VIII. p 89.

These large scale convective patterns modulate the local microturbulence amplitude as well. The root-mean-square fluctuating poloidal electrical field amplitude is shown in Fig.3. The data indicate that the turbulent electric field fluctuations are largest at the interface between adjacent large-scale convective patterns. This suggests that the convective patterns are a driving source for the turbulent fluctuations. In this scenario, the large-scale convective patterns decay and generate small-scaled vortices which are damped as they propagate away from the excitation region. Additional analysis and measurements are needed to confirm this physical picture.

Large-scale convection is the dominant particle transport mechanism inside the limiter radius in CCT. At the limiter radius both turbulent particle transport and large scale convection are important transport processes. In the scrape-off layer, turbulent transport is the dominant particle transport mechanism. In CCT the total radial transport of particles varies significantly with poloidal position. Variations in the local density and electron temperature that correspond to the local radial transport rate are also observed.

These results indicate that flux-surface averaged pictures of transport present a limited view of tokamak transport. Additional measurements in CCT are needed to study the origin of the convective cells and to confirm the relationship between large scale convection and small scale plasma turbulence. Two-dimensional flow visualization techniques should be tried in CCT to make a direct observation of the convective patterns. A search for similar convective patterns in other tokamaks is also being planned and initial experiments will be performed on the TEXTOR tokamak during late 1991 and early 1992. If such patterns are found in TEXTOR, then large-scale convection may prove to be an important transport mechanism that exists in all tokamak devices.

Relevant publications

- [1] G.R. Tynan, "Two-dimensional particle transport in the CCT tokamak edge plasma UCLA-PPG-1369, June 1991.
- [2] G.R. Tynan et al. "Steady-state convection and fluctuation-driven particle transport in the H-mode transition" to be published in Phys. Rev. Lett.
- [3] G.R. Tynan et al. Bull. APS 36:9 2500(1991).
- [4] G.R. Tynan et al. Proc. on 18th Euro. Conf. on Controlled Fusion and Plasma Physics, June 1991 Berlin, FGR, VIII. p 89.

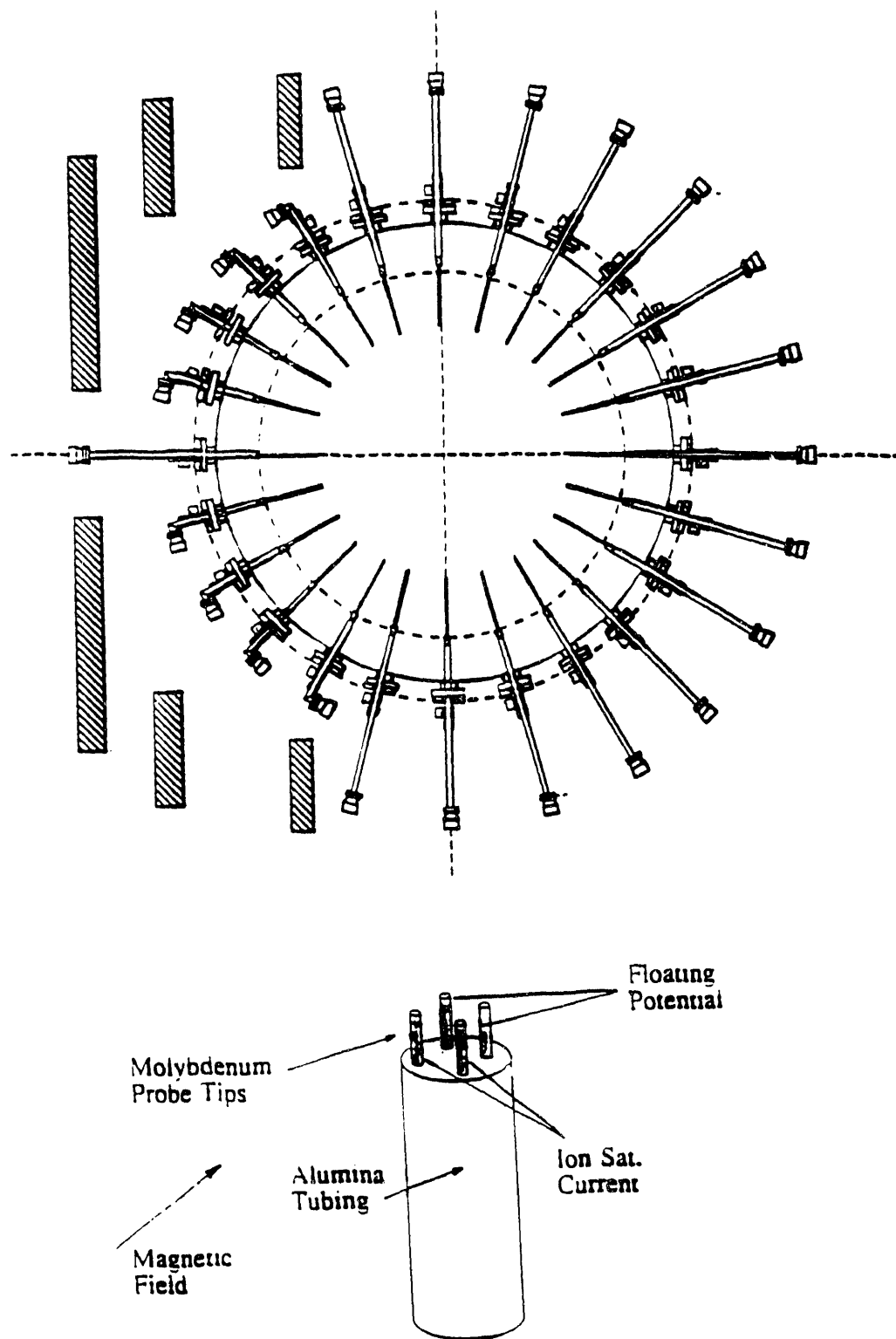


Figure 1: CCT Poloidal Probe Array and Probe Tip Details

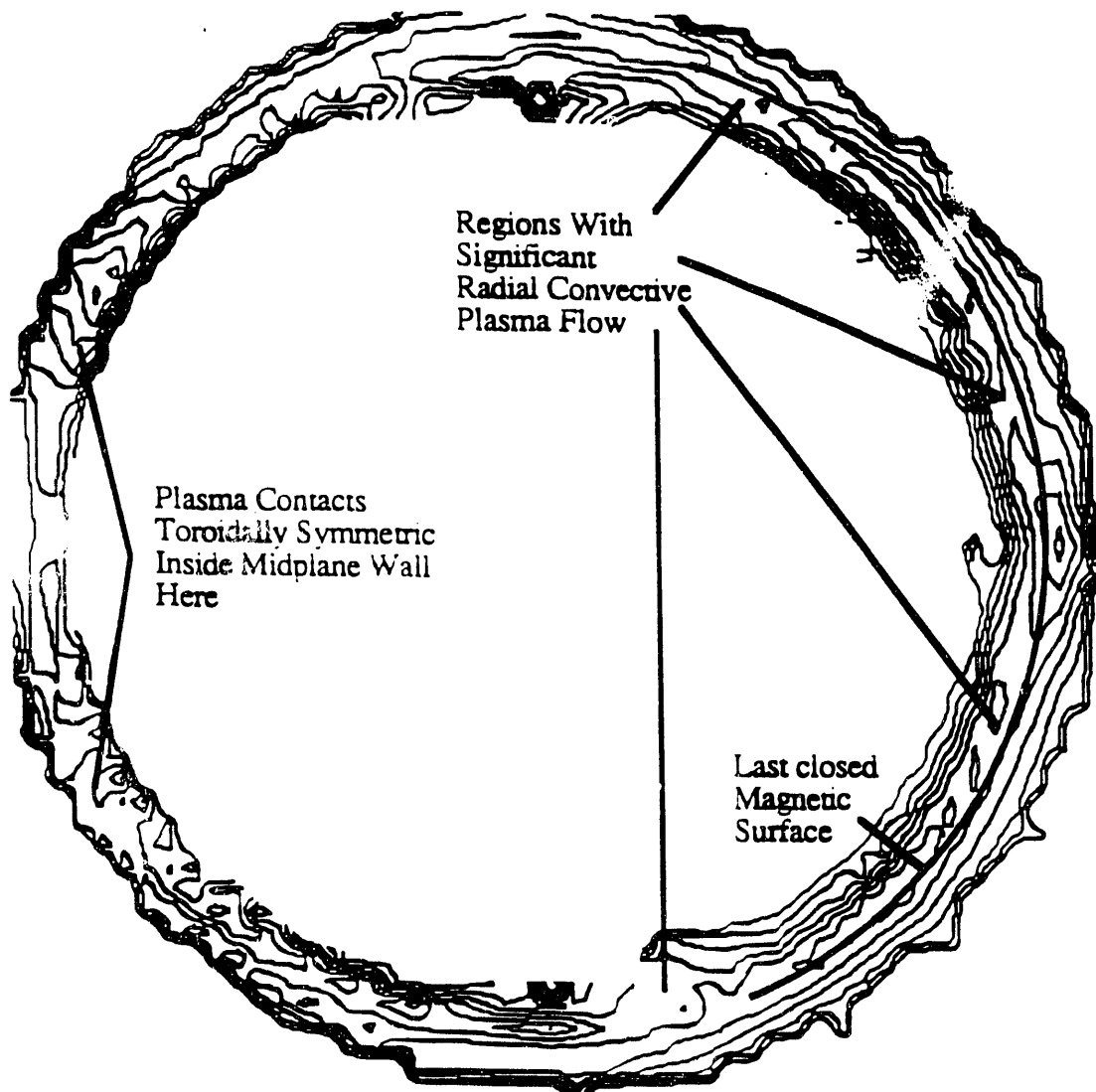


Figure 2: Time-averaged plasma potential radial and poloidal distribution in the edge plasma region of the CCT tokamak (15V contours shown). Outside midplane is to the right in the figure. Data from measured floating potential and electron temperature distribution. The results indicate the presence of large-scale stationary electric fields in the edge plasma region. These electric fields induce $E \times B$ plasma drifts in the radial and poloidal directions.

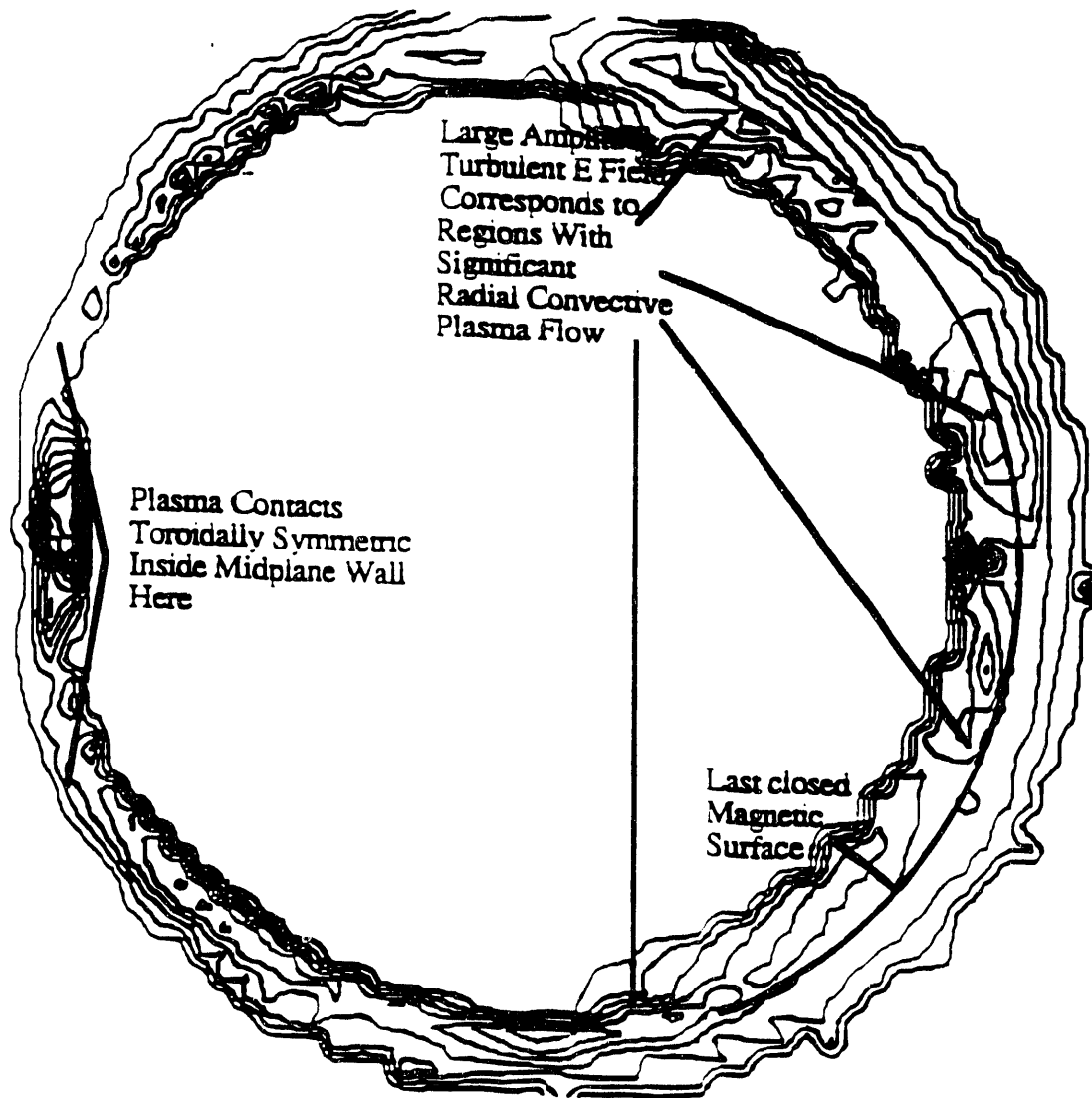


Figure 3: Radial and poloidal distribution of the root-mean-squared fluctuation poloidal electric field (4 V/cm contours shown). Outside midplane is to the right in the figure. The \bar{E}_θ amplitude is largest at the periphery of the convective patterns and at the interface between adjacent convective patterns. This suggests that the plasma turbulence is driven, at least in part, by the large-scale plasma flow.

H-Mode Transition Physics-I: Turbulent Transport Behavior

Ongoing research on the L to H mode transition in tokamaks has centered on the radial electric field as being the controlling factor in the transition. The magnitude of the electric field, or the strength of the shear in the field, can dramatically influence the nature of the electrostatic turbulence in the edge plasma. Furthermore, it has been suggested that the turbulent nature of the plasma controls the cross field heat and particle transport. Thus, the radial electric field can have a significant bearing on the rate of anomalous cross field diffusion.

PISCES provides a unique environment for studying the effects of radial electric fields on plasmas with conditions similar to tokamak edge plasmas. Steady state discharges are studied with probe arrays, either mounted on pneumatic carriages or fixed in the plasma dump. Spectroscopic means for monitoring the turbulence are also available. Because of the strong negative potential applied to the cathode in a reflex arc discharge, an inwardly pointing radial electric field is present even without an applied bias to the plasma periphery. Using an annular electrode mounted on a limiting aperture plate (Figure 1), the existing electric field can be modified and the peak electric field strength has been observed in excess of 100V/cm. The radial electric field is increased when a large electron current is drawn to the annular electrode. When this strong electron current is drawn, the radial electric field is peaked near the aperture radius (Figure 2a) and the central plasma density increases (Figure 2b). In addition, the density scrape-off length decreases significantly when the bias is applied. From the measured potential profiles, a poloidal flow profile can be inferred, and when the bias is not applied, a natural single shear layer exists just inside of the aperture radius. When the electron current is drawn, this layer is modified to a double shear layer, with a strong jet of plasma rotating poloidally just inside the aperture radius.

The nature of the turbulence and the turbulent driven particle flux also change dramatically between the single and double shear layer cases. In the double shear layer case, both the density and potential fluctuation levels decrease in the scrape-off layer (Figures 2c-d), while the density fluctuation levels are not modified significantly in the central plasma column. The turbulent driven particle flux is inferred from the strength and phase between the fluctuating poloidal electric field and density. Temperature fluctuations are not taken into account and are considered negligible. The turbulent driven particle flux is decreased by 30 to 90% when the double shear layer is formed (Figure 2e), due mostly to a suppression of the turbulence rather than a change in the phase between the density and electric field fluctuations. From a spectral analysis of the potential fluctuations

from the poloidally separated probes, as well as a radially staggered probe, both the poloidal and radial correlation lengths at the aperture radius are seen to decrease when a double shear layer exists. This suggests that small turbulent eddies are being stretched and torn in the strong poloidal jet that forms when the bias is applied.

Future work will include a search for coherent fluctuations using conditional sampling techniques. Scalings of the turbulent properties with neutral pressure, magnetic field, and electric field strength and shear are continuing. The ongoing edge plasma modelling effort at UCLA continues to use data provided by PISCES.

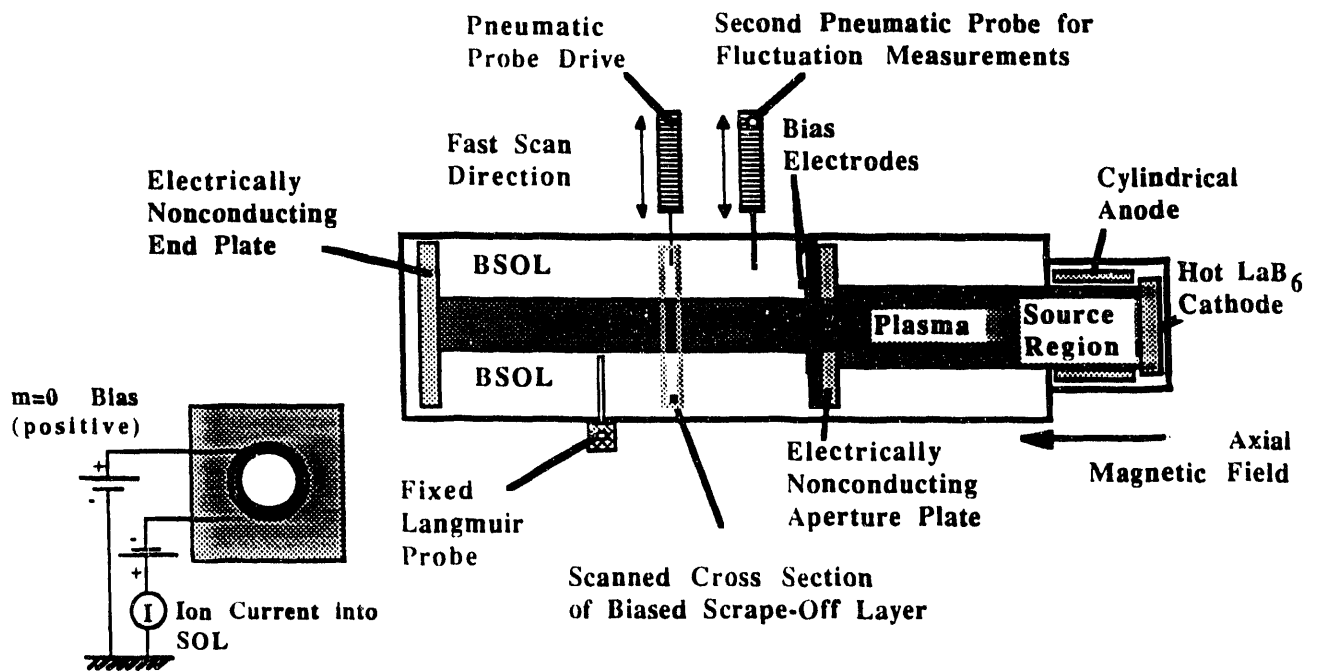


Figure 1: Schematic diagram of the experimental setup for the bias experiments in PISCES-A.

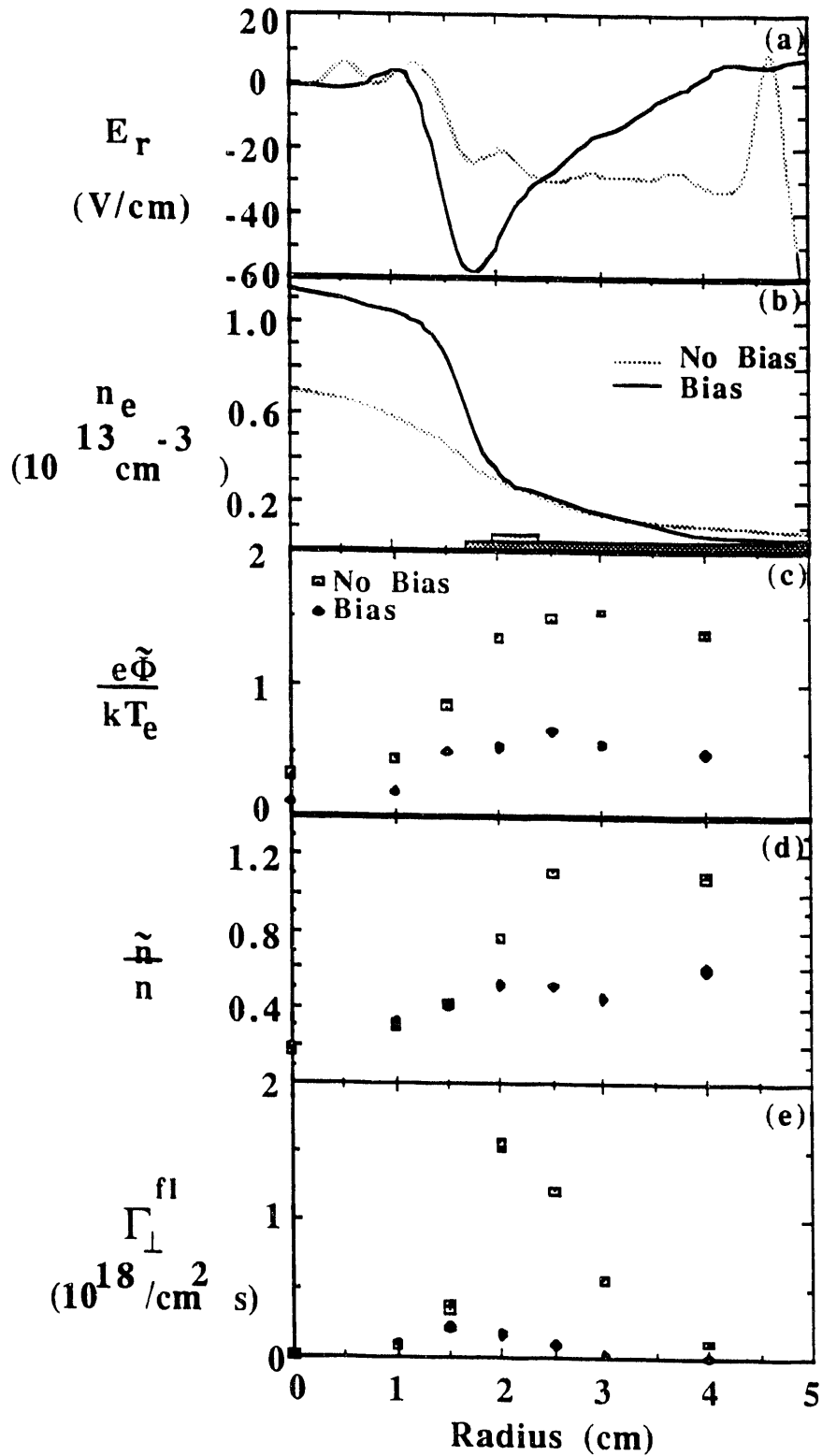


Figure 2: Radial profiles comparing unbiased and strongly biased conditions: (a) radial electric field, (b) plasma density, (c) potential fluctuations, (d) density fluctuations, and (e) turbulent-driven particle flux.

H-Mode Transition Physics-II: Observation of Steady State Convection

Turbulent fluctuations are not the only mechanism that has been proposed to control the cross field heat and particle transport in tokamak edge plasmas. It has been conjectured that steady state or long lived coherent structures may be responsible for some of the poloidal asymmetries observed in tokamaks. These coherent structures can also contribute to the particle and heat transport through non-diffusive transport processes such as convection. In addition, the convective patterns can also stimulate electrostatic turbulence, which in turn produces turbulent driven transport. Since convective patterns are difficult to map out, studying them under controlled conditions may shed some light on their contribution to heat and particle transport, as well as the L to H mode transition.

Convective patterns can be studied under the same conditions as the turbulence experiments described previously. Steady state discharges in PISCES are scanned with a pneumatic fast scanning probe mounted on a sliding O-ring seal. Two dimensional profiles of the plasma potential and density are created by accumulating successive shots while moving the probe carriage perpendicularly to the axis of the plasma column. The strength of the radial electric field can be modified by applying a bias to an annular ring electrode just outside of the aperture radius. Figure 1 shows the two dimensional plasma potential and density profiles when no bias is applied to the annular electrode. Because of the strong negative potential applied to the cathode in a reflex arc discharge, the potential in the central region of the discharge is depressed. Since the equipotential and equi-density contours are not cylindrically symmetric outside of the central plasma column, large scale, steady state convective cells are seen to be present. Figure 2 shows the same two dimensional profiles when a strong electron current is drawn to the annular electrode and a stronger radial electric field is produced. The contour plots show that the poloidal asymmetries in the potential and density are minimized when the stronger radial electric field is applied. The reduction of poloidal asymmetries coincides with a decrease in turbulence levels and reduction in the total radial particle transport.

Future work will concentrate on visualizing convective patterns with both a grid of Langmuir probes and conditional sampling techniques. Improvements in the control and stability of the discharge will be made to minimize shot to shot variations that limit the resolution of the existing experimental technique. Changes in convective cell structure due to changes in edge density gradients and the shear in the radial electric field will be studied to better understand the impact on transport barrier formation during tokamak H-modes.

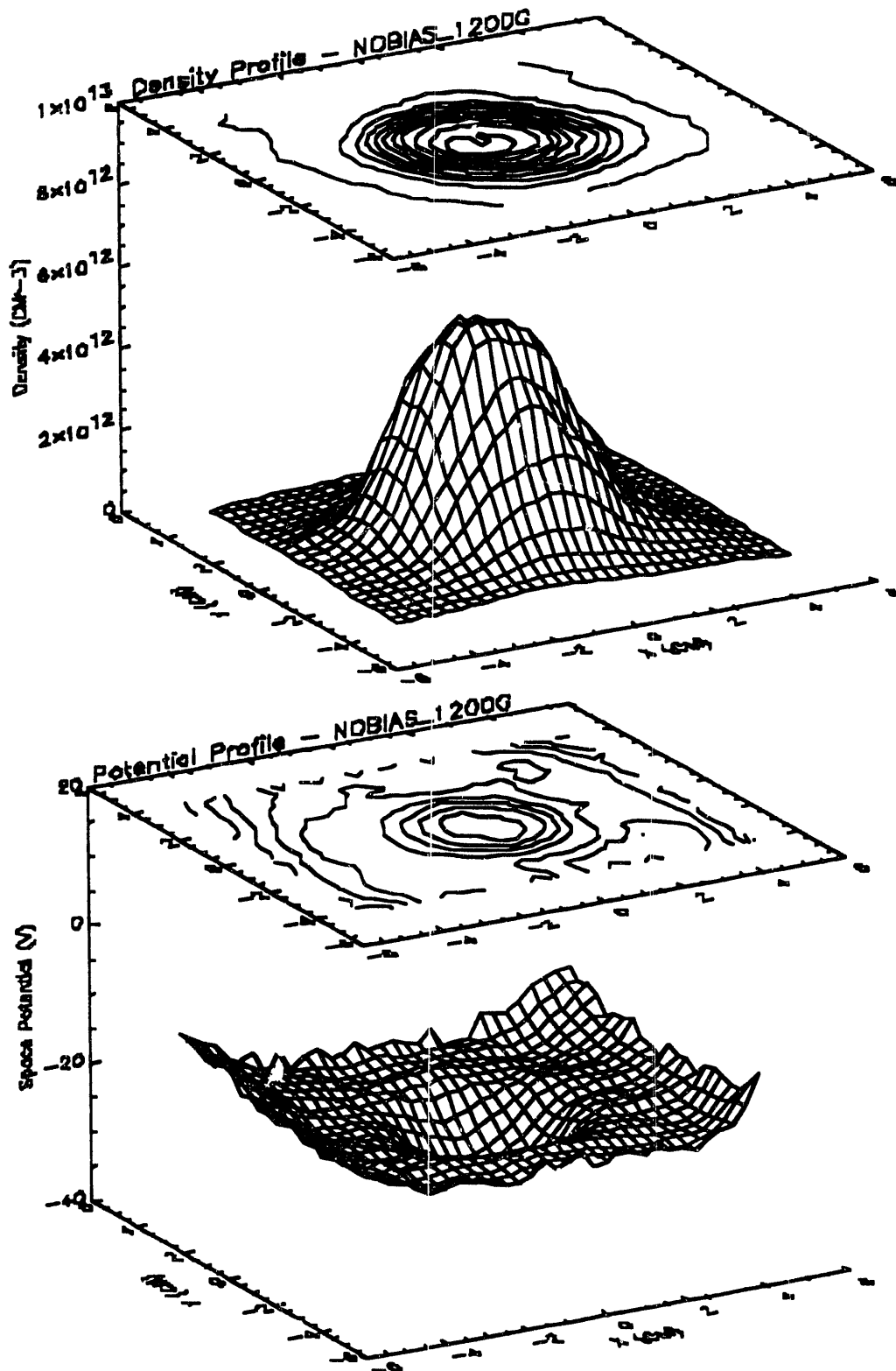


Figure 1: Density and potential profiles without biasing. Poloidal asymmetries are observed in both the density and potential profiles.

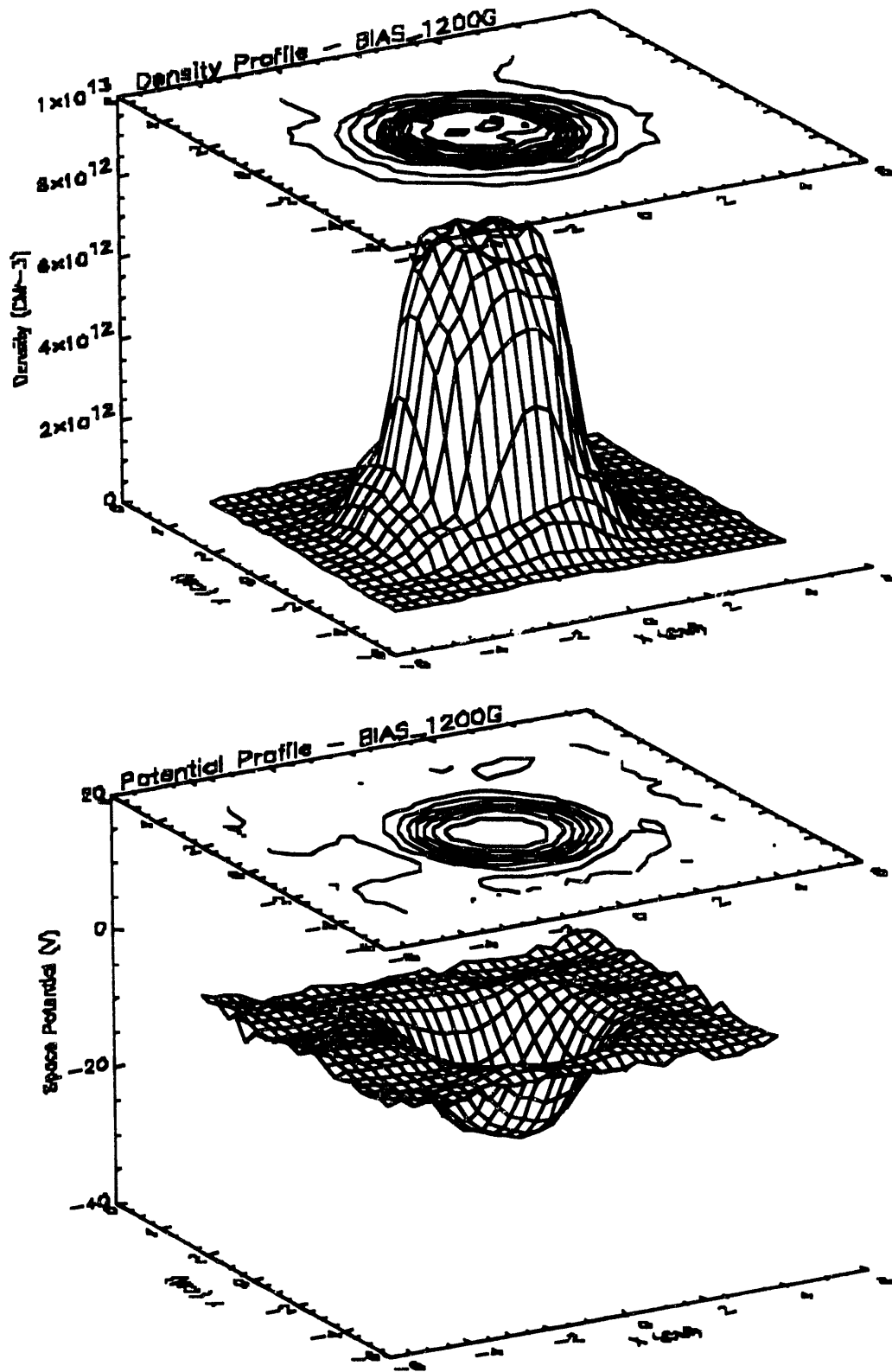


Figure 2: Density and potential profiles during strong biasing. Density and electric field profile in scrape-off layer steepen and poloidal asymmetries are minimized.

5. Theoretical Analysis

- Edge Plasma Modelling -

H-mode Physics-III: Plasma Behavior in a Sheared Electric Field

Recent tokamak H-mode experiments indicate that a strong radial electric field is formed at the plasma edge during the transition between L-mode and H-mode confinement. This radial electric field is radially localized in a narrow region and leads to a highly sheared $\underline{E} \times \underline{B}$ plasma flow. Simulation experiments currently being performed in the PISCES-A linear device, indicate that the fluctuation level and fluctuation induced particle transport are reduced when a strong, double shear layer (DS) is produced by biasing the plasma boundary layer, whereas the turbulence level and transport is rather high in the case of a weak single shear layer (SS) (observed when no bias is applied).

The source of the turbulence in SS cases is thought to be the Kelvin-Helmholtz instability (K-H), since the results of the experiments have shown some characteristic properties of this instability. Considering that larger shear and two shear layers are the major differences between the DS and SS cases, the following analytical and numerical simulation work is being performed to understand the dominant physics involved in these experiments.

(1) The kinetic equilibrium of plasma in a strongly sheared electric field

Since the driving source for the K-H is the sheared flow of plasma rather than the sheared electric field, correct information about the plasma response to a sheared electric field is needed. Usually, a plasma (in a uniform magnetic field B_z) is thought to respond with a steady state $\underline{E} \times \underline{B}$ drift to an electric field. This is true for the case where the electric field is uniform and weak, and the time scale of interest is much larger than the ion gyro-period. However, the plasma responds in a different way if the electric field has a large spatial gradient or the time scale of interest is shorter than the ion gyro-period.

A set of implicit expressions is derived for the motion of a single ion in an arbitrarily sheared electric field (the field and its gradient in x-direction are prescribed). The motion of an ion in a highly sheared electric field is evaluated numerically. When a linear spatial variation of an electric field is considered, the plasma has the following response. (a) if the gradient of the electric field is in the +x direction, the motion of an ion is always periodic but with a larger frequency (called 'shear gyro-frequency' in this report), which is the sum of the gyro-frequency and the 'shear frequency' (defined as the gradient of the $\underline{E} \times \underline{B}$ drift velocity). The concept of periodic motion around a drifting guiding center still applies, but the drift speed is different from normal the $\underline{E} \times \underline{B}$ drift speed (very different if the shear frequency is comparable to the gyro-frequency). For the purpose of investigating the K-H instability, approximation of a steady drifting plasma equilibrium with the new drift velocity is roughly valid. (b) If the gradient of the E-field is in the -x

direction, the motion of an ion is very different from the $\underline{E} \times \underline{B}$ drift motion. The ion may experience no drift, or drift in a direction opposite to the normal $\underline{E} \times \underline{B}$ drift. In our DS experiments, one of the two shear layers exhibits this behavior.

(2) Interaction between two K-H unstable regions

If a steady $\underline{E} \times \underline{B}$ drift is assumed to be the response of plasma to an electric field, a double shear layer implies two sheared plasma layers with sheared flow and each layer will drive a K-H type instability. Thus two K-H instabilities will be driven initially in DS cases, while only one will exist in the SS case. To understand the effect of the interaction between the two regions, a linear analysis has been done using a fluid model. The results show that for nonsymmetric double shear layers, this effect reduces the growth rate of the K-H instability driven in the layer with the larger shear frequency while increasing the growth rate of the other K-H mode. For symmetric double shear drift layers, the growth rates of both K-H modes are reduced, and the effect is more significant. More detailed analysis of such interaction is under way by means of a particle simulation.

(3) Particle simulation

Since we are dealing with a nonuniform, bounded plasma, and have to take into account significant effects from the finite shear frequency and finite Larmor radius effects, an analytical approach is insufficient. And since we wish to understand the nonlinear behavior of the plasma for comparison with experimental results, a fluid model clearly is not sufficient. Therefore we analyze the problem by means of a particle simulation, which preserves kinetic effects. The BEPS-2D code, written by Dr. Decyk of the UCLA Physics Department, has been modified to simulate these physical processes. The code is capable of analyzing electrostatic plasma behavior in two dimensions. Modifications include (a) the initial density can be nonuniform; (b) an SS or DS electric field can initially be entered and the electron density profile will automatically be adjusted to satisfy Poisson's equation; (c) plasma can be nonneutral; (d) the equilibrium electric field can be maintained during the entire simulation; (e) the initial velocity distribution function is Maxwellian with a superimposed local drift speed. Convective cells driven by $m=2$ and $m=3$ K-H modes have been observed during test runs of this code for weak double shear layer cases. The results will be compared with the PISCES-A experimental results and should provide additional insight into the physics of cross-field plasma transport in highly sheared plasma flow layers.

Anomalous Boundary Plasma Transport by Subharmonic Electric Fields

In the gaseous divertor experiment in PISCES-A, it has been observed that the effective radial diffusion coefficient increases with increasing neutral gas density but is independent of the magnetic field in the range explored so far (< 0.2 T). The effective radial diffusion coefficient is larger than the Bohm coefficient and the classical ambipolar diffusion coefficient. It is postulated that the turbulent electrostatic fluctuations observed during the experiments may be responsible for this enhanced anomalous transport phenomenon. This theoretical analysis is intended to investigate the motion of a charged particle in a uniform magnetic field perturbed by an electrostatic field.

Depending on the magnitude of the perturbation, the particle motion can range from a small deviation from simple cyclotron motion to stochastic motion over the whole phase space. The latter case corresponds to anomalous transport. Thus, by studying the interaction between the particle motion and the perturbative electric field we may gain deeper insight into the particle transport mechanism.

The classical equation of motion for a single particle gyrating around a magnetic field line has periodic analytical solutions. If the particle motion is perturbed by an electric field, then the particle motion may no longer be described by a closed analytical expression. Instead, depending on the strength of the perturbation, the particle may exhibit stochastic motion in phase space (x - v space). An example is the so-called "kicked oscillator" with Hamiltonian [1]

$$H = \frac{x^2}{2} + \frac{\omega_0^2 x^2}{2} - \varepsilon \frac{\omega_0^2}{k} \cos kx \sum_{n=-\infty}^{\infty} \delta(t - n T_0) \quad (1)$$

(where the mass is set to unity, ε is a dimensionless perturbation parameter, $T_0 = 2\pi/\Omega$ is the fundamental perturbation period and Ω is the fundamental perturbation frequency). Equation 1 corresponds to the motion of a charged particle in a uniform magnetic field in the z -direction with cyclotron frequency ω_0 , and under the influence of the wave packet field traveling along the x -axis.

The evolution of Eq. (1) in phase space can display many interesting phenomena. For example, if the resonance condition is satisfied ($\Omega/\omega_0 = \text{integer}$), i.e., in the harmonic case, a stochastic web structure with an exponentially thin width for small values of perturbation strength appears [1], and this web structure extends throughout the whole phase space. A particle originally located within the stochastic web will diffuse along the stochastic web and may reach distant parts of the phase space [3]. This phenomenon, the so-called Arnold diffusion [2], is the most unexpected discovery in the theory of non-integrable Hamiltonian systems. Particles starting from low energy can be accelerated to

very high energy through interaction with a wave packet of limited energy. The subharmonic case ($\omega_0/\Omega = \text{integer}$), however, has not yet been investigated in detail.

The goal of the present work is to investigate the particle motion under the influence of a subharmonic field, i.e., the particle motion perturbed by a wave field with a frequency that is some fractional part of the ion cyclotron frequency. This case is frequently encountered in the tokamak boundary plasma. We consider the one-dimensional motion of a particle described by the equation

$$\ddot{x} + \omega_0^2 x = \frac{E_0}{m} \sin(kx - \Omega t) \quad (2)$$

which describes particle motion under the influence of a perturbation field with frequency Ω , perpendicular to a uniform magnetic field. By making an independent variable transformation $\tau = \omega_0 t$, we can normalize the time to the cyclotron period. The equation of motion then becomes

$$\ddot{x} + x = \varepsilon \sin(kx - n\tau) \quad (3),$$

where $\varepsilon = e E_0 / m \omega_0^2$ is the perturbation strength of the electrostatic field and $n = \Omega / \omega_0$ is the ratio of the perturbation frequency to the cyclotron frequency.

Figs. 1-3(a) show the trajectories of a particle in phase space as a function of time (x, v vs. t ($= 0$ to 48π) plot). In Fig. 1-3(b), we show the phase trajectories in each cyclotron period superimposed in one cell for twenty-four consecutive periods (x, v vs. t ($= 0 - 2\pi$)). Fig. 1 is the phase plot of the unperturbed case, that is, $\varepsilon = 0$, and as we expect, the particle just exhibits simple harmonic motion. Fig. 2-3 show the numerical solutions of Eq. (4) with $\varepsilon = 0.1$ and $k = 1$. Fig. 2(a) shows that the harmonic electric field only slightly perturbs the cyclotron orbit, while in Fig. 3(a) the subharmonic electric field strongly pushes the trajectory away from the circular motion. This point is illustrated more clearly in Figs. 2-3(b). In Fig. 2(b), the particle motion traces out almost the same trajectory every 2π , while in Fig. 3(b) the trajectory breaks into four bands with finite widths. Due to this finite band width, the particle motion becomes stochastic. The position of the particle after a finite number of cyclotron periods can no longer be predicted accurately.

These results suggest that for the same parameters and perturbation strength, the subharmonic field can perturb the phase trajectory more effectively than the harmonic field. Therefore, the observed subharmonic electric fluctuations may greatly contribute to the anomalous particle transport in our experiments.

-
- [1] V.V.Afanas'ev et.al. Phys.Lett.A151(1990)276.
 [2] V.I.Arnold, "Mathematical Methods of Classical Mechanics", Springer-Verlag, NY, 1989.
 [3] G.M.Zaskavsky et.al. "Weak Chaos and Quasi-Regular Patterns", Cambridge Press, 1991.

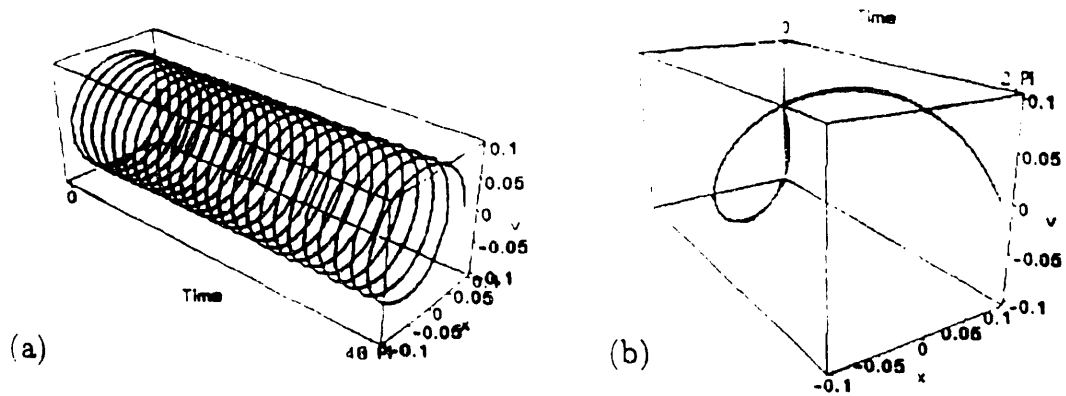


Figure 1: The cyclotron motion of a charged particle gyrating around a magnetic field line, with $\omega = 1$, $\Omega = 4$, $\varepsilon = 0$, and $k = 1$. The initial conditions are $(x_0, v_0) = (0.1, 0)$. Starting from $t = 0$ to 48π .

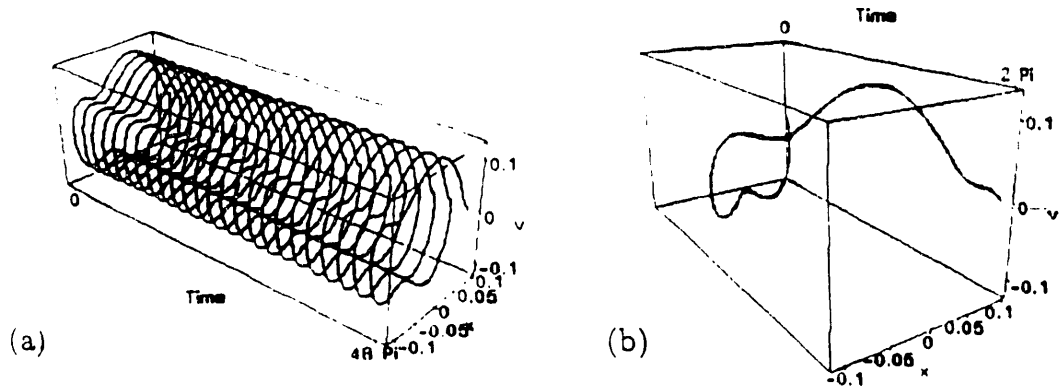


Figure 2: The particle motion under the influence of perturbative harmonic electric field with $\Omega = 4$ and $\varepsilon = 0.1$.

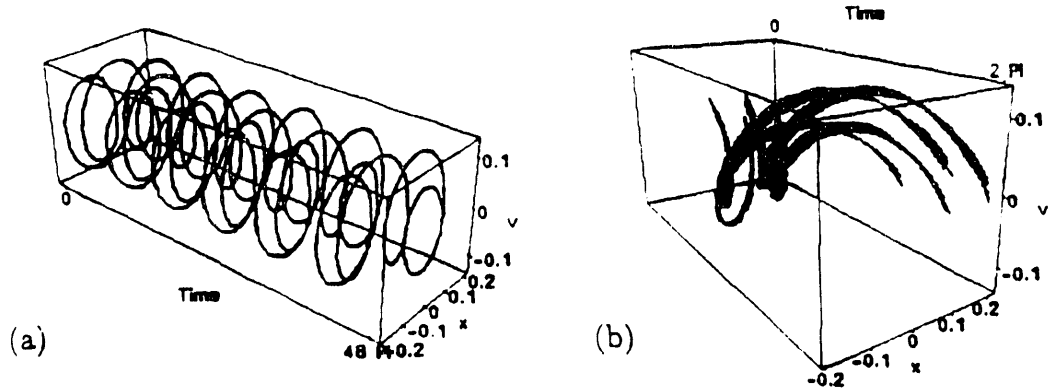


Figure 3: The particle motion under the influence of perturbative subharmonic electric field with $\Omega = 1/4$ and $\varepsilon = 0.1$.

END

**DATE
FILMED**

1 / 29 / 93

